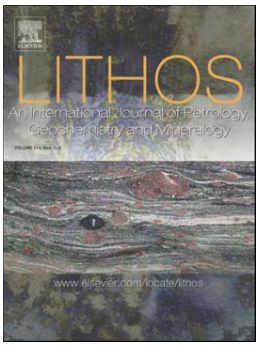

Platinum-group elements and gold in sulfide melts from modern arc basalt (Tolbachik volcano, Kamchatka)

M. Zelenski, V.S. Kamenetsky, J.A. Mavrogenes, L.V. Danyushevsky, D. Matveev, A.A. Gurenko

PII: S0024-4937(17)30290-6
DOI: doi:10.1016/j.lithos.2017.08.012
Reference: LITHOS 4395

To appear in: *LITHOS*

Received date: 30 May 2017
Accepted date: 21 August 2017

Please cite this article as: Zelenski, M., Kamenetsky, V.S., Mavrogenes, J.A., Danyushevsky, L.V., Matveev, D., Gurenko, A.A., Platinum-group elements and gold in sulfide melts from modern arc basalt (Tolbachik volcano, Kamchatka), *LITHOS* (2017), doi:10.1016/j.lithos.2017.08.012

Platinum-group elements and gold in sulfide melts from modern arc basalt (Tolbachik volcano, Kamchatka)

M. Zelenski [a], V.S. Kamenetsky [a,b,*], J.A. Mavrogenes [c], L.V. Danyushevsky [b], D. Matveev [d], A.A. Gurenko [e]

[a] *Institute of Experimental Mineralogy RAS, Chernogolovka 142432, Russia*

[b] *Earth Sciences and CODES, University of Tasmania, Private Bag 79, Hobart, TAS 7001, Australia*

[c] *Research School of Earth Sciences, Australian National University, Canberra, ACT 2601, Australia*

[d] *Institute of Solid State Physics RAS, Chernogolovka 142432, Russia*

[e] *Centre de Recherches Pétrographiques et Géochimiques (CRPG), UMR 7358, Université de Lorraine, 54501 Vandoeuvre-lès-Nancy, France*

* Corresponding author.

E-mail address: Dima.Kamenetsky@utas.edu.au (Vadim Kamenetsky)

ABSTRACT

Sulfide melt inclusions entrapped in primitive olivine phenocrysts can be used to understand the compositions of early sulfide melts that may ultimately contribute to magmatic sulfide ore deposits. Sulfide globules hosted in olivine (86-92 mol% Fo) from the Tolbachik basalt (the 1941 eruption) are characterized in terms of their major and trace element abundances using electron microscopy and LA-ICP-MS analysis. Distribution of major elements within individual sulfide globules varies from homogeneous to heterogeneous. Phases include monosulfide solid solution (MSS) and intermediate solid solution (ISS) intergrowths and exsolved low-temperature minerals such as pyrrhotite, pentlandite, chalcopyrite and cubanite. Trace elements (platinum-group elements - PGE, Ag, Te, Au, Pb and Bi) are also present in solid solution in sulfide phases and as micron-sized particles ("nuggets"). Such nuggets of dominantly Au, Pt, Au-Pd and Pd-Te are contained randomly within sulfide matrices or, more commonly, at phase boundaries. Nuggets are also attached to outer surfaces of sulfide globules. Concentrations of PGE in sulfides follow a log normal distribution over four orders of magnitude. The highest measured noble metal

concentrations in the analyzed globules (436 ppm Au + PGE) are 133 ppm Au, 115 ppm Pt and 299 ppm Pd, whereas 40% of globules have < 15 ppm of noble metals. Gold and PGE concentrations correlate, suggesting these elements were concentrated by the same process(es). We propose that a number of anomalous concentrations of one or several noble metals in the analyzed globules can be best explained by entrapment of Au-PGE-rich particles (solid or liquid) from the silicate melt. Although the individual Tolbachik sulfide globules have variable PGE abundances, their mean composition resembles those of major PGE-sulfide ore deposits (e.g., Norilsk, Sudbury, Platreef and Merensky Reef).

1. Introduction

A remarkable feature of magmatic sulfide ores is their high concentrations of platinum-group elements (PGE) and gold, which may exceed corresponding concentrations of these elements in parental silicate liquids by 3-5 orders of magnitude (Barnes and Ripley, 2016; Campbell and Barnes, 1984; Naldrett, 2004). Accumulation of PGE-Au in sulfide melts derived by liquid immiscibility relies on efficient diffusive transport of metals from cogenetic silicate melts (Barnes and Ripley, 2016; Mungall, 2002; Zhang, 2015), and is the end result of complex interactions of a number of processes. As diffusion of metals in silicate melt is relatively slow, even at magmatic temperatures (Zhang et al., 2010 and references therein), and with PGE-Au abundances at sub-ppb to ppb levels (e.g., Bezos et al., 2005; Meisel and Moser, 2004; Naldrett, 2004), noble metal enrichment of magmatic sulfide liquids requires sufficiently long interaction of the latter with large volumes of silicate melt, even with extremely high sulfide/silicate partition coefficients. Nevertheless, the modern theories of sulfide ore deposit formation consider diffusion as the main process responsible for concentration of trace elements (Au-PGE) in sulfide liquid (e.g., Campbell and Barnes, 1984; Naldrett, 2004). Concentrations of PGE in sulfide melt can be further upgraded by direct entrapment of micron- and submicron-sized PGE-containing particles (which include pure metals, PGE alloys, sulfides, bismuthinides, etc.) that may be present in primitive magmas prior to

and during sulfide segregation. Although the existence of such nano- and micro-particles of PGE minerals (PGM) in silicate melts has been directly confirmed (Kamenetsky et al., 2015; Park et al., 2012) and suggested in a number of works (e.g., Andrews and Brenan, 2002; Anenburg and Mavrogenes, 2016; Tredoux et al., 1995), collection of such particles by growing sulfide droplets is yet to be recognized.

Massive or disseminated magmatic sulfide ores cannot provide reliable evidence for physical incorporation of early particles of PGE from the silicate melt into magmatic sulfides due to their high solubility in sulfide liquids (e.g., Fonseca et al., 2009; Pruseth and Palme, 2004). Also, magmatic and post-magmatic processes erase original compositions of incipient sulfide droplets. Such processes include coalescence of sulfide droplets at the base of magma chambers (averaging compositions), recrystallization of deposited sulfides, entrainment of sulfide melts by new batches of magma and alteration caused by syn- and post-magmatic fluids. On the other hand, sulfide droplets entrapped and quenched in early magmatic minerals (e.g., olivine and Cr-spinel) represent the least modified compositions of immiscible sulfide melts. Importantly, these globules contain numerous noble-metal nuggets, which crystallized from the sulfide melt upon cooling, but also could have been trapped from magma by sulfide droplets (e.g., Holwell et al., 2015; Holwell et al., 2011; Kamenetsky et al., 2013; Kamenetsky et al., 2015).

In this study, droplets of sulfide melt (sulfide globules) sealed in primitive olivine phenocrysts from island arc magma (high-Mg basalts produced by the 1941 eruption of Tolbachik volcano) reveal high concentrations of noble metals. We report the occurrence and overall abundances of noble metals and their alloys and minerals in immiscible sulfide melt. We also show that the high PGE content of sulfides could be acquired, at least partially, by direct capture of PGE-rich phases by growing sulfide droplets from the silicate magma.

2. Tolbachik volcano

The Tolbachik Volcanic Complex in the central part of the Central Kamchatka Depression is the southernmost of the Klyuchevskoy Group of volcanoes, which are located at the north

termination of the Kuril-Kamchatka arc in in the northwest Pacific. Two major volcanoes, Ostry Tolbachik and Plosky Tolbachik, form a single massif with a highest point at 3680 meters a.s.l. (55.8319 °N, 160.3272 °E). Two linear chains ("rift" zones) of more than 170 monogenetic cones extend NE and SSW from Plosky Tolbachik (Fig. 1). All recent activity was confined to the terminal caldera of Plosky Tolbachik and SSW "rift" zone, where three historic eruptions occurred with a total volume of ~2.2 km^3 of basalt (dense rock equivalent; Zelenski et al., 2016). The magmatic system of the Tolbachik volcano was reviewed by Belousov et al. (2015). Chemical compositions and petrographic features of Tolbachik rocks can be found in several publications (e.g., Churikova et al., 2015a; Churikova et al., 2015b; Flerov et al., 1984; Portnyagin et al., 2007; Portnyagin et al., 2015).

The rocks of Tolbachik belong either to medium- or high-K series, both with a relatively narrow interval of SiO_2 contents from basalts to basaltic trachyandesites (Fig. 2a). Both series have bimodal MgO distributions that range from 3 to 5.5 wt.% MgO and from 8 to 11.5 wt.% MgO (Fig. 2b). The bimodal MgO content of Tolbachik rocks was attributed to extreme fractional crystallization (Flerov et al., 1984) or the product of two different mantle sources (Churikova et al., 2015b; Dosseto et al., 2003; Nikulin et al., 2012). The existence of the high-K series was attributed to mantle upwelling due to intra-arc rifting (Churikova et al., 2015b). Alternatively, the compositions of the Tolbachik volcanic series with an anomalously broad range (5–8-fold) of concentrations of incompatible elements (K, Rb, Nb, Ba) at a given MgO content fits a Recharge-Evacuation-Fractional Crystallization model (Portnyagin et al., 2015). The low values of $^{87}Sr/^{86}Sr$ (0.70334 – 0.70339; Churikova et al., 2015b; Dosseto et al., 2003; Portnyagin et al., 2015) indicate negligible assimilation of silicic crustal material.

3. Samples and Methods

Samples for this study were collected from the 1941 eruptive cone (summit at 55.7949° N, 160.3321° E, 2104 meters a.s.l.), 3.5 km SW of the edge of the summit caldera of Plosky Tolbachik (Supplementary Fig. 1, 2; Supplementary Table S1). Three samples of scoria ~ 10 kg each, and four

bulk samples of volcanic bombs and lava, ~ 15 kg each were crushed for bulk analysis and mineral separation. Major and trace element contents in rock samples were analyzed by XRF and ICP-MS in the Geoscience Laboratories, Sudbury, Ontario. Gold and PGE contents in rock samples were analyzed using NiS fire assay pre-concentration and the tellurium co-precipitation technique followed by ICP-MS (Geoscience Laboratories, Sudbury, Ontario).

Samples of lava and scoria were crushed, sieved and the olivine fraction was separated by heavy liquid with a specific gravity of 3.0 (bromoform + methylene iodide). Olivine crystals with sulfide globules were picked from a Petri dish under immersion liquid and examined under binocular microscope. In order to determine unbiased compositions of sulfide melts and exclude random variability caused by later crystallization of distinct phases, ~ 60 olivines containing sulfide globules were reheated to 1200 °C and quenched in water. Crystals containing globules (typically ≥ 50 μm) were mounted in epoxy resin and polished to expose included sulfide. Each crystal was placed in a separate 6 mm epoxy mount and ground to expose sulfide globules at a middle-plane level. Individual mounts were then placed into 1-inch standard mounts. Such technique allows studying representative globules at their mid-plane exposed areas.

Several dozen sulfide globules were extracted intact by complete dissolution of host olivine crystals in 48% hydrofluoric acid at ~60 °C. After extraction, whole sulfide globules were mounted on carbon film and studied by electron microscope similar to polished globules.

3.1. In-situ Energy-Dispersive Spectroscopy

Exposed surfaces of sulfides globules were photographed in reflected light and studied under electron microscope with Energy-Dispersive Spectrometer (Vega Tescan II XMU, Institute of Experimental Mineralogy, Russian Academy of Sciences, Chernogolovka, Russia; Hitachi SU-70, Central Science Laboratory, University of Tasmania, Hobart). Analyses were performed using either a rastered beam over the whole exposed surface to obtain the bulk composition of each globule (Table 2, Supplementary Tables S4a-c), or with a focused beam to analyze individual

phases. Volume concentrations of major elements were also measured in19 globules by LA-ICP-MS analysis. Considering the fine-grained texture of the majority of globules, the rastered beam provided values close to the bulk (volume) composition even for visually heterogeneous, multiphase globules, where surface (EDS) and volume (LA-ICP-MS) estimates of the composition returned similar results (Supplementary Fig. S3). The following analytical conditions were applied during EDS analysis: accelerating voltage 15 or 20 kV, probe current 300-400 pA, spot size 100–200 nm. Standards used for EDS measurements in Chernogolovka are listed in Supplementary Table S2. Standardless EDS analysis was done in Hobart. To increase accuracy and precision of EDS measurements and to decrease detection limits, long counting times, up to 600 s excluding dead time were used for some critical measurements, which provided detection limits for most of elements and precision of measurements of around 0.05 wt.% (2σ or confidence level 95%).

3.2. LA-ICP-MS analysis

LA-ICP-MS analyses were performed at CODES Analytical Laboratories, University of Tasmania. The instrumentation involved an ASI RESOLution-LR-S155 laser microprobe equipped with a Coherent Compex-Pro 193 nm Ar-F excimer laser, coupled to an Agilent 7700s quadrupole ICP-MS. A laser beam size of 50 micron was used with a pulse rate of 5 Hz and a fluence of 2.7 J/cm^2. Ablation was performed in a He atmosphere flowing at 0.35 L/min. The ablated aerosol was mixed with Ar (1.05 L/min) as a transport gas, before exiting the cell. Tuning was performed to minimize oxides (<0.15 % ThO/Th) and maximize sensitivity for the mid and high mass isotopes.

The following isotopes measured were: ^{34}S, ^{57}Fe, ^{59}Co, ^{60}Ni, ^{65}Cu, ^{66}Zn, ^{99}Ru, ^{101}Ru, ^{103}Rh, ^{105}Pd, ^{106}Pd, ^{107}Ag, ^{111}Cd, ^{125}Te, ^{185}Re, ^{189}Os, ^{193}Ir, ^{195}Pt, ^{197}Au, ^{206}Pb and ^{209}Bi. Arsenic was not among analyzed elements because a preliminary study of the sulfide globules by EDS showed no presence of this element. Dwell time was 5 ms for S, Fe, Pb and Bi, 10 ms for Ag and 20 ms for all other elements, resulting in a total sweep time of 0.346 sec. Total acquisition time for each analysis was 90 seconds, consisting of 30 seconds gas background and 60 seconds ablated signal.

Quantification was performed following the standard methods (Košler, 2001; Longerich et al., 1996). Calibration involved STDGL2b2 (Danyushevsky et al., 2011), NIS3 (Gilbert et al., 2013) and Po724-T (Sylvester et al., 2005) reference materials, and Fe as the internal standard element. Instrumental drift was corrected by hourly analyses of references materials across the analytical session. Due to the unknown bulk composition of the sulfide inclusions, quantification involved normalization to 100 wt.% total.

Corrections for base metal-argide interferences are required for the quantification of Ru, Rh and Pd by LA-ICP-MS techniques (Guillong et al., 2011; Sylvester, 2001). The analysis of magmatic sulfides has the potential to form $^{61}Ni^{40}Ar$ interferences on ^{101}Ru, $^{59}Co^{40}Ar$ on ^{99}Ru, $^{63}Cu^{40}Ar$ on ^{103}Rh, $^{65}Cu^{40}Ar$ on ^{105}Pd, and $^{66}Zn^{40}Ar$ on ^{106}Pd. For the quantification of Ru, Rh and Pd, the extent of base metal-argide production was determined by ablating pure Ni, Cu, Zn and Co metals and a correction factor applied to the results. All ^{106}Pd results were corrected for isobaric interference from ^{106}Cd, which was monitored by recording the signal on ^{111}Cd.

4. Results

4.1. Rocks of the 1941 Tolbachik eruption

The 1941 lavas and scoria are high-K magnesian basalts with 50.5-51.0 wt.% SiO_2, 8.9 wt.% MgO, 1.35 wt.% K_2O and Mg# 62–64 (Table 1, Supplementary Table S3). According to Portnyagin et al. (2015), the 1941 Tolbachik basalt has hybrid compositions resulting from mixing between high-Mg/mid-K and low-Mg/high-K magmas. The rocks contain ~ 4 wt.% phenocrysts, the majority of which are euhedral olivine crystals 1-5 mm in size, with normal zoning from cores of Fo_{88-92} to rims of Fo_{80-85}. Plagioclase, pyroxene and Cr-spinel phenocrysts are rare. The groundmass comprises olivine, clinopyroxene, plagioclase, Ti-magnetite and interstitial glass. In terms of trace elements (Supplementary Table S3), samples from the 1941 eruption belong to one of two trends, both of which are systematically enriched (by a factor of two) in LILE, HFSE and REE relative to N-MORB (Churikova et al., 2015b).

All studied olivines collected from the 1941 Tolbachik eruption are from: (1) tephra with basaltic glass attached to surfaces, containing glassy inclusions, (2) volcanic bombs and (3) thick basalt flows. Olivine grains underwent cooling at different rates, from rapid (in tephra) through intermediate (in bombs) to slow (in lava).

Olivine crystals contain numerous melt inclusions (MI), 20–100 μm in size, rarely up to 300 μm. Many MI from loose olivines and scoria are naturally quenched and contain glass and a shrinkage bubble, with or without daughter phases. Compositions of MI, corrected for in-situ olivine crystallization, are more primitive, but still overlap with the whole rock MgO contents (8-13 and 8.9 wt.%, respectively; MI study in progress). However, the compositions of MI and host basalts cannot be linked by simple fractional crystallization of common phenocrysts, as the abundances of K_2O (0.50-0.85 and 1.35 wt.%, respectively), P_2O_5 and trace element ratios (e.g., Sr/Nd, Ba/Rb, Zr/Hf, Zr/Sm etc.) are principally different. MIs contain variable amounts of volatiles, up to 5.1 wt.% H_2O, 1200 ppm CO_2, 0.35 wt.% S and 0.28 wt.% Cl (H_2O and CO_2 contents measured by SIMS in CRPG, Nancy, Kamenetsky et al., 2017). Some glasses, associated with sulfides, have exceedingly high sulfur contents (up to ~ 1.0 wt.% S), at the upper limit measured in arc magmas (see review in Wallace and Edmonds, 2011).

4.2. Tolbachik sulfides

Approximately 0.6 % of the olivine grains from the 1941 Tolbachik basalts contain entrapped sulfide melt globules (Fig. 3). Many globules are nearly spherical, which establishes them as captured liquids. Some globules are flattened or elongated along crystallographic axes of the host crystal, or have irregular shape. Globules are typically 10-100 μm in size, rarely reaching 250 μm. No sulfides have been observed within the rock groundmass.

The rate of cooling of the olivine phenocrysts varies greatly from very rapid (in lapilli) to relatively slow (in lava). Depending on the quench rate, the texture of sulfide globules can be visually homogeneous (Fig. 3a), or fine- to coarse-grained intergrowths of various Ni-rich and Cu-rich phases (Fig. 3b, c, 5a), or consist of crisscrossing lamellae of individual sulfides (Fig. 3d). The

other factor influencing the composition of sulfides is the size of the globule. Small globules lack nucleation sites and tend to be undercooled, which leads to fine-grained textures (e.g., Patten et al., 2012).

Most globules contain crisscrossing intergrowths of chalcopyrite ($CuFeS_2$), cubanite ($CuFe_2S_3$) and rarely bornite (Cu_5FeS_4), associated with "patches" of Ni-rich phase $(Fe,Ni)_9S_8$ (pentlandite or mackinawite) and non- stoichiometric Ni-rich and Cu-rich phases (Fig. 3b – d) that possibly correspond to MSS (Fe-Ni-S monosulfide solid solution) and ISS (Fe-Cu-S intermediate solid solution). Heated and quenched globules demonstrate homogeneous textures for Fe-rich, Ni-rich and Cu-rich sulfides (Supplementary Fig. S4a – c) and fine-grained textures in sulfides containing approximately equal amounts of Ni and Cu (Supplementary Fig. S4d).

The compositions of individual sulfide globules plot in the Fe–Ni–Cu–S–O quinary system. The amount of oxygen is not more than a few percent and is concentrated in low-Ti magnetite. Assuming a metal to sulfur ratio close to unity (Me:S = 0.938 ± 0.075 (2σ) and 0.998 ± 0.076 (2σ) for unheated and heated samples, respectively), all compositions of the Tolbachik sulfides plot in a FeS–NiS–CuS ternary, where each point represents the average composition of the exposed surface area of individual globules (Fig. 4).

The majority of the compositional data plots within the FeS–0.5NiS–0.5CuS ternary. The maximum measured contents of NiS and CuS are 38.1 and 37.6 mol%, respectively. High Cu contents in sulfides may reflect elevated Cu in the 1941 Tolbachik magma (160-280 ppm Cu, Table 1, Supplementary Table 3). Highly variable Ni/Cu ratios (0.1-35 and 0.08–120 for unheated and heated globules, respectively) were most likely caused by variability of Ni and Cu contents in the parent magma, reflected in variable Ni and Cu contents in olivine (study in progress), whereby sulfide-free olivine crystals contain more Ni than sulfide-bearing crystals. Compositional variability of heated and unheated sulfide globules is similar, although the field for unheated globules is marginally wider.

4.3. Noble metal phases in sulfides

Some sulfide globules contain minute phases composed of high atomic number elements (Pd, Ag, Te, Pt, Au, Pb and Bi) and thus are easily recognized by back-scattered scanning electron microscopy (Fig. 5, 6). These grains (hereafter referred to as "nuggets" due to their size, typically < 0.5 μm) are found alone or in clusters on exposed surfaces (both natural and exposed by polishing) of sulfide globules. The majority of such nuggets apparently formed in-situ as a result of fractional crystallization of the sulfide melt during cooling. However, in some cases, as advocated below, the presence of nuggets can be attributed to direct entrapment from the ambient silicate melt and/or saturation in noble metals caused by selective dissolution of sulfide droplets (see Sections 5.3 – 5.4).

4.3.1. Appearance and spatial distribution of nuggets

Nuggets vary in size from < 100 nm to 3 μm, with the majority falling in the range of 200-500 nm. The smallest nuggets are round or elliptical in shape, which most likely reflects random Gaussian distribution of back-scattered electrons rather than real shapes. Larger nuggets often demonstrate tabular, needle-like or complex shapes, especially those located in caverns in the sulfide matrix (Fig. 5b). The largest nugget ~3 μm across was found on the outer surface of a sulfide globule (Fig. 6a).

The number of nuggets on exposed surfaces of globules varies from one to several dozen, depending on the scale of observation (Fig. 6d). With one exception, nuggets are observed in globules ≥ 20 μm in diameter. Nuggets may be randomly scattered over a globule in cross-section, but some are confined to pits in the polished surfaces (Fig. 5b) and boundaries between Ni- and Cu-rich phases (Fig. 5e, f), or attached to outer surfaces of globules (Fig. 6a-c).

4.3.2. Composition of nuggets

The small size of nuggets hinders accurate determination of compositions by energy-dispersive spectrometry (EDS), because the analytical volume (at an accelerating voltage of 15 keV, specimen

density ~ 4.5 g/cc) is around 1–1.2 μm across, which greatly exceeds the size of most nuggets. The smallest nuggets could not be analyzed. Semi-quantitative compositions of nuggets ≥ 200 nm can be estimated by subtracting matrix elements (Fe, Ni, Cu, S and O) from the analyses. As a result, 200+ analyzed nuggets listed in Table 3 yielded 45 combinations of Pd, Ag, Te, Pt, Au, Pb and Bi (Supplementary Tables S5a, S5b). The number of observed nuggets is much greater than the number analyzed. At higher magnifications, nuggets smaller than 0.1-0.3 μm become detectable, but their size renders quantification impossible.

The list of inferred phases (Table 3) includes four pure metals (Ag, Pt, Au and Pb), 16 binary, 17 ternary, and 8 more complex combinations of metals. Although Ru, Os and Ir are present in sulfides in measurable amounts (see Section 4.4), they were not confidently detected in nuggets. Accurate deciphering of nuggets is challenging because their analyses include matrix elements. For example, a nugget denoted as "Ag" could be native silver, acanthite Ag_2S, argentopyrite $AgFe_2S_3$, frieseite $Ag_2Fe_5S_8$, lenaite $AgFeS_2$, argentopentlandite $Ag(Fe,Ni)_8S_8$, stromeyerite AgCuS, mckinstryite $Ag_{5-x}Cu_{3+}xS_4$, or an unknown mineral, or aggregates of several phases. Gold nuggets are likely native gold, but could be auricupride Cu_3Au or tetra-auricupride CuAu. In most cases the neighboring nuggets show diverse compositions and morphology (Fig. 5, 6). We found no correlation between the compositions of the sulfide matrix (i.e. Fe-Ni or Fe-Cu) and included nuggets.

Platinum (23 occurrences), gold (18) and Au-Pd alloys (16) are the most abundant native metals among studied nuggets. Pd-Te is the most common binary compound with a Pd/Te ratios similar to those in keithconnite $Pd_{20}Te_7$ and kotulskite Pd(Te,Bi). The latter was reliably analyzed in the largest observed nugget (Fig. 6). Palladium is by far the most abundant element in nuggets, and 190 of 207 measured compositions include Pd, Pt, or Au. Fourteen nuggets are solely composed of Ag or Pb, however, considering the high affinity of these elements to sulfur, the Ag- and Pb-bearing nuggets are likely Ag_2S, PbS, or more complex sulfide minerals also containing Fe, Ni or Cu.

An extraordinary case of abundant large Pd-Pt particles is recorded in a sulfide globule only 7.5 μm in diameter. Eighteen nuggets of dominantly PdPt and Pd_4Pt and a distinct sulfide phase containing 38 wt.% Pt, 7 wt.% Rh and 4 wt.% Pd together with 13 wt.% Cu are present in this globule (Fig. 7). Rhodium, Pd and Pt account for ~25 wt.% of the globule. The analyzed values provide only a rough estimate of the real composition of these tiny phases, because interferences from neighboring minerals cannot be excluded.

4.4. Trace element compositions of sulfide globules

Nineteen sulfide globules in olivine (Supplementary Fig. S8) were analyzed using the LA-ICP-MS technique to determine concentrations and distribution of highly siderophile elements (Au, Re and PGE), semi-metals (Te) and chalcophile trace metals (Zn, Ag, Cd, Re, Pb, and Bi). Major elements of the sulfide matrix (Fe, Ni, Co, Cu and S) were also measured in the LA-ICP-MS analyses. The sulfide globules were exposed at around the mid-plane level by careful polishing, examined by optical and electron microscope, and analyzed for major elements by EDS. The globules containing nuggets on their polished surfaces were targeted first; another selection criterion for the laser ablation analysis was a broader range of major element compositions in terms of Fe:Ni:Cu ratios (Fig. 4). More than 50 % of the volume of globules was analyzed by laser ablation. Fourteen globules accommodated a single analytical spot, whereas five globules were large enough for two (3) and three (2) analyses.

The concentrations measured in sulfide (rounded to 3 significant digits) together with basic statistics are given in Table 4; raw analytical data is provided in Supplementary Table S6. With few exceptions, all 19 analyzed elements were detected in each analytical spot. The behavior of the elements during analysis was monitored using time-resolved laser ablation spectra (hereafter, TRLAS; Fig. 8). These were used to determine if sulfides are homogeneous “down hole” (i.e. constant element ratios in the ablated volume), and if they contain nuggets large enough to be recorded.

The majority of single point analyses demonstrate homogeneous major element compositions, however, in some cases variable Ni/Cu can be seen in TRLAS (e.g., #2-6, #8-9 and #12-5; Fig. 8d, f, g). The variations in major elements can be accompanied by corresponding changes of some chalcophile elements; for example Zn and Ag in relation to Cu and Ni, respectively (#8-9 and #2-6; Fig. 8d, f).

Comparison of the major and trace element compositions of duplicate analyses show a range of homogeneity; two globules are homogeneous (#2-3 and #1-4), with max/min ratios <1.5 for all elements; two globules are moderately homogeneous (#3-3 and #13-7) with respect to all elements except Rh and Au; and one globule (#13-8) is heterogeneous. The major element compositions measured by LA-ICPMS mimic those analyzed by EDS on exposed surfaces and represent the whole compositional spectrum (Fig. 4, Table 2; Supplementary Fig. S3). Approximately half of the TRLAS reveal homogeneous distributions of trace elements (e.g., #2-3, #8-9 and 10-2; Fig. 8e, f, h), suggesting that either nuggets are too small to contribute signal or are not present. The other half of the TRLAS shows abrupt changes in intensities of certain elements (#13-7a, 12-2, 2-6 and 12-5; Fig. 8a, c, d, g) that are interpreted as nuggets. Nuggets recorded by TRLAS most commonly contain Au, Ag, Pt and Pd (#13-7a, 12-2 and 2-6; Fig. 8a, c, d). This is consistent with compositions of nuggets observed on polished surfaces (Fig. 5, Table 3). Globule #13-7 contains a Pd-Pt-Au-Bi phase(s) (Fig. 8a), a composition not previously observed by electron microscopy. Some analyzed globules with no visible nuggets contain nuggets at depth (e.g., #12-2 and #2-6; Fig. 8c, d). Although the contribution from nuggets is included in the calculation of bulk sulfide compositions, the highest abundances of Pd, Pt, Pb and Bi and appreciable amounts of other PGE, Au and Ag are recorded in the completely homogeneous globule #2-3 (Fig. 8e), which has a smooth TRLAS (i.e. no nuggets). Similarly, PGM nuggets were not detected in globule #8-9 (Fig. 8f), which contains 10-1000 times higher concentrations of Rh, Os and Ir than any other globules. Nuggets are also not recorded in globule #10-2, which is characterized by the highest Re content, but is the most

depleted in all other trace elements (Fig. 8h). The smooth TRLAS seen in globule #1-4 reveals the highest Ag and modest abundances of Pd, Pt, Au and Te (Table 4).

5. Discussion

5.1. Noble metal nuggets in sulfide matrix

Some nuggets are scattered randomly within sulfide matrix (Fig 5b, 6d); others are confined to phase boundaries (Fig. 5e, f and Fig. 6e, f) or attached to outer surfaces of sulfide globules (Fig. 6a - c). Spatial position and nugget size are related. The smallest nuggets (< 100 nm, Fig. 6d) are randomly distributed within sulfide matrix, while larger nuggets (0.2–3 μm) occur along boundaries between Ni-rich and Cu-rich phases (Fig. 5f, 6e, f), and at the surface of globules (Fig. 6a). The average contribution of nuggets to the total content of noble metals in sulfide can be calculated, given their number, size and composition. It is known that the total volume of objects per unit volume is equal to their total cross-sectional area per unit area on a typical plane section $V_V = A_A$ ("Delesse principle", e.g., Royet, 1991). For sulfide globules with abundant nuggets (such as shown in Fig. 5a-c), their total cross-sectional area was estimated at 0.02%. Therefore, the nugget volume density makes up to ~ 0.02 volume% or ~ 0.07 wt.% of the sulfide. This provides the total contribution of 320 ppm Pd, 120 ppm Pt and 240 ppm Au. The inferred contributions of Pt and Pd matches the highest concentrations of these elements measured by LA-ICP-MS in the homogeneous sulfide globules (299 ppm Pd and 115 ppm Pt). The estimated gold content (240 ppm Au) exceeds the maximum measured (37 ppm Au) by a factor of six. These calculations show that submicron nuggets in sulfide globules can make a significant contribution to noble metal contents.

5.2. Statistics of element concentrations in sulfide globules

Measured abundances of chalcophile and highly siderophile elements in sulfide globules vary by two to four orders of magnitude, with the exception of S, Fe, Co (max/min = 1.2 to 2.4), Zn (3.5) and Ni (11). In contrast, Ir and Bi concentrations have max/min ratios ~ 10000. The highest measured total PGE and Au is 436 ppm (# 2-3, Fig. 8e, Table 4), which includes 299 ppm Pd, 115

ppm Pt and 13 ppm Au, while several sulfide globules contain only a few ppm of noble metals. No significant statistical difference in measured concentrations of metals was observed between homogeneous and heterogeneous sulfide globules or between sulfide globules with or without nuggets, either visible under SEM or detected by LA-ICP-MS. This suggests that most nuggets (except the extraordinary case shown in Fig. 7) were exsolved from the sulfide melt upon cooling and solidification.

Basic statistics of elemental concentrations (max, min, range, mean, median and mean to median ratio) are provided in Table 4. The mean to median (M/M) ratio is a simple indicator of the degree of inequality in distribution, i.e., how far from normal a population is. The mean is affected by a few or even a single anomalous measurement, whereas the median is insensitive to "outliers". In normal distributions the mean and median values are equal. M/M ratios for all elements except Re and PGE are in the range of 0.882 – 1.57. Not surprisingly, the two most abundant elements (sulfur and iron) have M/M ratios close to unity (0.996 and 1.02, respectively). M/M ratios for chalcophile trace metals (Zn, Cd, Pb, Bi) are all less than unity (0.932 to 0.961) indicating that some measurements of these elements were low. On the other hand, M/M ratios for Re (3.52) and PGE (3.13 – 12.5) are well above unity, indicative of high concentrations in one to three globules.

Concentrations of PGE in the Tolbachik sulfides follow a lognormal distribution, i.e. the logarithms of the concentrations show a normal distribution (Fig. 9a–c). Because of a limited number of analyses, a characteristic bell-shaped distribution of Pd and Os is not obvious (Fig. 9a, b). However, if we put all PGE together and normalize the total amount of each element to 100%, the resulting distribution of log of the concentration is near normal (Fig. 9c). Lognormal distributions of element concentrations indicate that a major fraction of a given noble metal is present in only a few sulfide globules. For example, a single globule #8-9 (Fig. 8f, Table 4) contains more Os and Ir than all other 18 analyzed globules taken together, considering element concentrations and globule volumes. The lognormal distribution also means that abundances of

noble metals in sulfides are much greater than their modal (most frequent) concentrations. Concentrations of chalcophile elements, except Zn, show bimodal distributions (Fig. 9d).

The lognormal distribution, which is "*a fundamental law of the distribution of the concentration of an element...*" (Ahrens, 1954), is generated by many random effects that are multiplicative. In our case, such random factors contributing to concentrations of PGE in the sulfide liquid include: (1) the concentration of an element in the silicate melt; (2) the duration of interaction between silicate and sulfide melts; (3) the degree of supersaturation of the silicate melt in respect to sulfide C^{FeS}_0, when growth of sulfide droplets is imposed by low diffusion flux of S^{2-}, and the apparent R factor (Campbell and Naldrett, 1979) is proportional to the reciprocal of C^{FeS}_0 (kinetic control of sulfide composition, Mungall, 2002). The concentration of an element in the silicate melt is probably the most stable variable. The duration of sulfide-silicate interaction is unknown, but may vary significantly (minutes to years, e.g., Zhang, 2015). The reciprocal of C^{FeS}_0 (and therefore the apparent R factor) can vary the most, because it changes from a relatively small value to infinity when the level of sulfide supersaturation approaches zero.

5.3. Evidence for the presence of Au-PGE-rich phases in silicate melt

Clearly, the complex interplay of factors responsible for the lognormal distributions of element concentrations equally affects all metals. In fact, the concentrations of measured PGE and gold correlate well if anomalous concentrations of one or several noble metals (outliers) are excluded. This is graphically illustrated in Fig. 10, where binary variation diagrams of Au, Rh, Pd, Os and Ir vs. Pt are presented. After eliminating outliers, correlations between these elements vary from 0.87 to 0.995 (R^2 = 0.76 - 0.99).

Another way to represent metal intercorrelations in analyzed sulfides is a bubble diagram (Fig. 11). Bubble areas here are proportional to concentrations of metals in individual sulfide globules; all globules are arranged in order of increasing gold concentration. The latter was selected as a reference element because of its high solubility in silicate melts, which ensures predominantly diffusive acquisition of gold by sulfide liquid. The concentrations of the chalcophile elements Zn

and Cd are approximately the same in most globules (see also Fig. 10f), supporting their equilibrium partitioning by diffusion from the magma. Zinc and Cd have such low partition coefficients $D = C_{sul}/C_{sil}$ that they reach a limiting concentration at almost any R factor. In contrast, the abundances of PGE are far from equilibrium, since at $D = C_{sul}/C_{sil}$ of around $10^5 – 10^6$ or higher (e.g., Barnes and Ripley, 2016; Fonseca et al., 2009; Mungall and Brenan, 2014) and $C_{sil} \sim 0.3 – 8$ ppb, the equilibrium concentrations of PGE in a sulfide liquid should reach 1000's of ppm.

Excessive concentrations of IPGE (globules #8-2, 8-9 and 9-7) and gold (globule #2-6), compared to common trends (Fig. 10) contrast with the systematics of these elements in the majority of analyzed sulfide globules. In particular, in #8-9 the Ru content is ~10^3 times and Os and Ir contents are ~10^2 times higher than expected. Such excess cannot be easily explained within the framework of the diffusion-controlled accumulation of noble metals. As an alternative, we propose the incorporation of pre-existing noble metal phases from the silicate melt in the sulfide globules. For example, for the 100-μm globule #8-9 the excessive concentrations of Ru (22.2 ppm), Rh (3.15 ppm), Os (7.7 ppm) and Ir (10.4 ppm) can be explained by fortuitous entrapment of a 3-μm crystal of laurite $(Ru,Rh,Os,Ir)S_2$ or aggregate of laurite with Os-Ir alloy. After incorporation, PGE-rich phases dissolved into the sulfide melt because of the extremely high solubilities of these elements in such melts (e.g., Fonseca et al., 2009; Fonseca et al., 2011; Pruseth and Palme, 2004). Globules #8-2 and 9-7 also contain appreciable amounts of excessive Rh and Ir (Table 4, Fig. 10 and 11) that can be accounted for by entrapment of Rh-Ir ± Os-rich phases directly from the silicate melt. Laurite was shown to be thermodynamically stable at magmatic temperatures ~1250 °C (Talkington and Lipin, 1986), whereas Ru solubility in basaltic melts at $fO_2 \leq$QFM can be lower than solubilities of other PGE (Borisov and Palme, 2000 and references therein). Crystallization of laurite directly from silicate melt has been confirmed by inclusions of laurite in early magmatic Cr-spinel (e.g., Kamenetsky et al., 2015).

It seems fortuitous for one trace phase in silicate melt (a microscopic noble-metal crystal) to encounter the other trace phase (sulfide globule). However, if we consider a different scenario

where PGE minerals (particles) in the silicate melt serve as nucleation sites for sulfide droplets (e.g., Mungall and Su, 2005; Patten et al., 2012) followed by coalescence of such droplets, it would be plausible that most PGE particles are ultimately incorporated in the sulfide melt. Alternatively, the PGE enrichment in conjugate sulfide – silicate melts may occur as "*the metallic PGE micro-alloys all fractionate into the sulfide liquid, where interfacial energies are lower*" (Ballhaus and Sylvester, 2000). Similarly, our data on PGE-rich phases associated with Tolbachik sulfide globules lend further support to the proposed ability of PGE to form "polyatomic metallic clusters" that, once formed, continuously coalesce into PGE-bearing phases (Anenburg and Mavrogenes, 2016; Ballhaus and Sylvester, 2000; Helmy et al., 2013; Tredoux et al., 1995). Experimentally demonstrated coalescence and growth of such phases on crystallizing phases such as magnetite and Cr-spinel (Anenburg and Mavrogenes, 2016; Finnigan et al., 2008) can be indicative of the same process occurring in silicate magmas undergoing sulfide immiscibility. This is strongly supported in recent studies of the Bushveld base metal sulfides in which "*a continuum …from discrete micrometer- to nanometer-sized*" PGM inclusions "*…precipitated from the silicate melt and afterwards were collected by the sulfide melt*" (Junge et al., 2015; Wirth et al., 2013).

5.4. Selective dissolution of PGE-bearing sulfide melt

Apart from direct crystallization of PGE minerals from silicate melt (e.g., Kamenetsky et al., 2015), other alternatives for the origin of PGE-rich particles can be: (1) PGE enrichment through selective dissolution of sulfide droplets, and (2) entrainment and dissolution of PGE-bearing mantle and crustal xenoliths.

Selective dissolution of sulfide droplets may take place in the course of their settling (or magma mixing), if a droplet drifts out of a reduced, sulfide-saturated ($C^{FeS}_0 > 0$) magma into another magma with less sulfur or/and more oxidized ($C^{FeS}_0 < 0$). This scenario seems plausible in the case of the 1941 Tolbachik magmas contaminated by external sulfur (Kamenetsky et al., 2017). If $C^{FeS}_0 < 0$, sulfide droplets experience selective extraction of FeS, whereas highly siderophile elements are being upgraded (Kerr and Leitch, 2005). This process can probably explain

anomalously high concentrations of Pd, Pt and Rh in the ~7-μm sulfide droplet shown in Fig. 7. At the exposed surface this droplet contains 18 individual grains of Pt-Pd alloys accounting for ~ 15 wt.% Pt or ~ 25 wt.% PGE in total. This droplet could form via selective dissolution of a large sulfide droplet with consequential enrichment of residual sulfide liquid in PGE, followed by exsolution of observed PGE phases. Therefore, such selective dissolution of a 150-μm sulfide droplet containing 16 ppm Pt (an average value for 19 measured Tolbachik sulfides, Table 4) may increase Pt content to ~15 wt.% after the droplet is reduced to 7 μm in diameter.

A similar process could have produced the PGE-nugget found in a melt embayment in olivine Fo_{83} (Fig. 12, Table 5, Supplementary Fig. S5-S7). The composition of this nugget (Table 5) corresponds to a mixture of Cu-Fe oxide (35-40 wt.%) and PGE-alloy containing all six platinum group elements (60-65 wt.%). The nugget probably originated from a sulfide droplet that contained appreciable amounts of PGE, but was subsequently oxidized and partially dissolved.

Another possible enrichment process can occur through dissolution of entrained mantle or crustal xenoliths, which are abundant in the 1941 Tolbachik basalt (study in progress). For example, residual sulfides in harzburgite mantle xenoliths from the Avachinsky volcano (Kamchatka) are highly enriched in Ir and Os (~30 ppm each, Bénard and Ionov, 2010); therefore, assimilation of similar rock lithologies in the Tolbachik magma may introduce IPGE nuggets and/or IPGE-rich sulfide droplets into the silicate melt. Similarly, entrapment of a miniscule particle of gold inherited from assimilated country rocks, (e.g., Zelenski et al., 2016) may explain anomalously high Au content in the globule #2-6 (Table 4, Fig. 11).

5.5. Can the Tolbachik sulfides be linked to magmatic sulfide ore deposits?

The origin of Au and PGE enrichment in large magmatic sulfide deposits is still controversial; both magmatic and hydrothermal-metasomatic processes have been invoked (Boudreau and McCallum, 1992; Campbell et al., 1983; Naldrett, 1997). Irrespective of their exact mode of deposition, the ultimate source of such extreme PGE enrichments must be PGE-bearing parental silicate melts capable of reaching sulfide saturation and efficient PGE capture in immiscible sulfide

liquids (Naldrett, 2010). Our study of high temperature immiscible sulfide melts and their PGE + Au budget provides an opportunity to shed light on the origin of and the concentration mechanisms of noble metals in the nascent stages of magmatic sulfide deposit formation.

Abundances of Au and PGE and metal ratios in the Tolbachik sulfides are comparable to those of some major sulfide ore deposits (Fig. 13b). Although the individual sulfide globules from the 1941 Tolbachik eruption are vastly different in terms of PGE abundances and PGE ratios, the mean sulfide composition diluted by a factor of ~3000 (3.5 orders of magnitude) defines the Au and PGE inventory of the 1941 Tolbachik basalt (Fig. 13a). Almost the same proportion was deduced for the Platreef (Holwell et al., 2011) and Merensky Reef (Ballhaus and Sylvester, 2000) in the Bushveld Complex. Additionally, similar phase relations and textures of base metal sulfides and compositions of noble metal phases in the Tolbachik case and Cu-Ni-PGE sulfide deposits are indistinguishable. Another outcome of our study is that liquids and alloys of noble metals in primitive magmas may impact modelling of the element partitioning between conjugate silicate and sulfide melts. However, we must also be aware that early crystallizing Cr-spinel (Arguin et al., 2016; Kamenetsky et al., 2015; Pagé and Barnes, 2016; Pagé et al., 2012; Park et al., 2012) can be responsible for depleting PGE concentrations prior to and during sulfide immiscibility.

6. Conclusions

1. Primitive island-arc magmas (Tolbachik volcano, Kamchatka) may undergo silicate-sulfide liquid immiscibility in the early stages of their evolution simultaneously with crystallization of high-magnesium olivine (Fo_{85-92}) and chrome spinel. Such sulfides may contain significant amounts of gold and PGE that are comparable to some prominent magmatic sulfide-PGE ore deposits, such as Norilsk, the Platreef and Merensky Reef. Sulfide droplets enclosed in olivine crystals are protected from external modifications, such as magma evolution, mixing, degassing and oxidation; thus they remain pristine magmatic.

2. Efficient diffusive transport of metals from cogenetic silicate melts is by far the main process responsible for the accumulation of PGE-Au in sulfide melts. However, observed

systematics of noble metal contents in the Tolbachik sulfides, namely, correlations between PGE contents and anomalous values (outliers), combined with high inequality of noble metal distributions, can be indicative of pre-existing PGM phases in the silicate melt. In particular, such particles may serve as nucleation sites for incipient sulfide droplets. Upon entrapment, PGM particles dissolve in the sulfide melt to provide high PGE tenors. Possible origins of such particles include their direct crystallization from the silicate melt and/or release from assimilated mantle and crustal xenoliths.

3. Upon cooling and crystallization, sulfide melts exsolve submicron-sized particles (nuggets) enriched in Au and PGE, dominated by native gold, native platinum, Au-Pd alloy and palladium tellurides. Although volume density of such nuggets does not exceed 0.02 %, high PGE tenors in some Tolbachik sulfides can be accounted for by their presence.

Acknowledgements

We thank Vasilii Yaschuk and Natalia Malik for their help in collecting samples, Maya Kamenetsky for sample preparation, Karsten Goemann, Sandrin Feig and Paul Olin for analytical work, and Maxim Portnyagin for useful comments. Rubén Piña, an anonymous reviewer and the editor Andrew Kerr provided useful comments that improved the text and presentation. This study was supported by the Russian Science Foundation grant #16-17-10145.

References

Ahrens, L.H., 1954. The lognormal distribution of the elements (A fundamental law of geochemistry and its subsidiary) Geochimica et Cosmochimica Acta 5, 49-73.

Andrews, D.R.A., Brenan, J.M., 2002. Phase-equilibrium constraints on the magmatic origin of laurite plus Ru-Os-Ir alloy. Canadian Mineralogist 40, 1705-1716.

Anenburg, M., Mavrogenes, J.A., 2016. Experimental observations on noble metal nanonuggets and Fe-Ti oxides, and the transport of platinum group elements in silicate melts. Geochimica et Cosmochimica Acta 192, 258-278.

Arguin, J.P., Pagé, P., Barnes, S.J., Yu, S.Y., Song, X.Y., 2016. The effect of chromite crystallization on the distribution of osmium, iridium, ruthenium and rhodium in picritic magmas: An example from the Emeishan Large Igneous province, Southwestern China. Journal of Petrology 57, 1019-1048.

Ballhaus, C., Sylvester, P., 2000. Noble metal enrichment processes in the Merensky Reef, Bushveld Complex. Journal of Petrology 41, 545-561.

Barnes, S.-J., Ripley, E.M., 2016. Highly siderophile and strongly chalcophile elements in magmatic ore deposits. Reviews in Mineralogy and Geochemistry 81, 725-774.

Belousov, A., Belousova, M., Edwards, B., Volynets, A., Melnikov, D., 2015. Overview of the precursors and dynamics of the 2012-13 basaltic fissure eruption of Tolbachik Volcano, Kamchatka, Russia. Journal of Volcanology and Geothermal Research 307, 22-37.

Bénard, A., Ionov, D.A., 2010. PGE and trace elements in veined sub-arc mantle xenoliths, Avachinsky volcano, Kamchatka. Geochimica et Cosmochimica Acta 74, A76.

Bezos, A., Lorand, J.P., Humler, E., Gros, M., 2005. Platinum-group element systematics in Mid-Oceanic Ridge basaltic glasses from the Pacific, Atlantic, and Indian Oceans. Geochimica et Cosmochimica Acta 69, 2613-2627.

Borisov, A., Palme, H., 2000. Solubilities of noble metals in Fe-containing silicate melts as derived from experiments in Fe-free systems. American Mineralogist 85, 1665-1673.

Boudreau, A.E., McCallum, I.S., 1992. Concentration of platinum-group elements by magmatic fluids in layered intrusions. Economic Geology 87, 1830-1848.

Campbell, I.H., Barnes, S.J., 1984. A model for the geochemistry of the platinum-group elements in magmatic sulfide deposits. Canadian Mineralogist 22, 151-160.

Campbell, I.H., Naldrett, A.J., 1979. The influence of silicate : sulfide ratios on the geochemistry of magmatic sulfides. Economic Geology 74, 1503-1506.

Campbell, I.H., Naldrett, A.J., Barnes, S.J., 1983. A model for the origin of the platinum-rich sulphide horizons in the Bushveld and Stillwater complexes. Journal of Petrology 24, 133-165.

Churikova, T.G., Gordeychik, B.N., Edwards, B.R., Ponomareva, V.V., Zelenin, E.A., 2015a. The Tolbachik volcanic massif: A review of the petrology, volcanology and eruption history prior to the 2012-2013 eruption. Journal of Volcanology and Geothermal Research 307, 3-21.

Churikova, T.G., Gordeychik, B.N., Iwamori, H., Nakamura, H., Ishizuka, O., Nishizawa, T., Haraguchi, S., Miyazaki, T., Vaglarov, B.S., 2015b. Petrological and geochemical evolution of the Tolbachik volcanic massif, Kamchatka, Russia. Journal of Volcanology and Geothermal Research 307, 156-181.

Danyushevsky, L., Robinson, P., Gilbert, S., Norman, M., Large, R., McGoldrick, P., Shelley, M., 2011. Routine quantitative multi-element analysis of sulphide minerals by laser ablation ICP-MS: Standard development and consideration of matrix effects. Geochemistry: Exploration, Environment, Analysis 11, 51-60.

Dosseto, A., Bourdon, B., Joron, J.-L., Dupré, B., 2003. U–Th–Pa–Ra study of the Kamchatka arc: new constraints on the genesis of arc lavas. Geochimica et Cosmochimica Acta 67, 2857-2877.

Finnigan, C.S., Brenan, J.M., Mungall, J.E., McDonough, W.F., 2008. Experiments and models bearing on the role of chromite as a collector of platinum group minerals by local reduction. Journal of Petrology 49, 1647-1665.

Flerov, G.B., Andreev, V.N., Budnikov, V.A., Tsyurupa, A.I., 1984. Petrology of the eruption products, in: Fedotov, S.A. (Ed.), The Great Tolbachik Fissure Eruption, Kamchatka, 1975-1976. Nauka, Moscow, pp. 223-284 (in Russian).

Fonseca, R.O.C., Campbell, I.H., O'Neill, H.S.C., Allen, C.M., 2009. Solubility of Pt in sulphide mattes: Implications for the genesis of PGE-rich horizons in layered intrusions. Geochimica et Cosmochimica Acta 73, 5764-5777.

Fonseca, R.O.C., Mallmann, G., O'Neill, H.S., Campbell, I.H., Laurenz, V., 2011. Solubility of Os and Ir in sulfide melt: Implications for Re/Os fractionation during mantle melting. Earth and Planetary Science Letters 311, 339-350.

Gilbert, S., Danyushevsky, L., Robinson, P., Wohlgemuth-Ueberwasser, C., Pearson, N., Savard, D., Norman, M., Hanley, J., 2013. A comparative study of five reference materials and the Lombard meteorite for the determination of the platinum-group elements and gold by LA-ICP-MS. Geostandards and Geoanalytical Research 37, 51-64.

Guillong, M., Danyushevsky, L., Walle, M., Raveggi, M., 2011. The effect of quadrupole ICPMS interface and ion lens design on argide formation. Implications for LA-ICPMS analysis of PGE's in geological samples. Journal of Analytical Atomic Spectrometry 26, 1401-1407.

Helmy, H.M., Ballhaus, C., Fonseca, R.O.C., Wirth, R., Nagel, T., Tredoux, M., 2013. Noble metal nanoclusters and nanoparticles precede mineral formation in magmatic sulphide melts. Nature Communications 4, 2405, 10.1038/ncomms3405.

Holwell, D.A., Keays, R.R., McDonald, I., Williams, M.R., 2015. Extreme enrichment of Se, Te, PGE and Au in Cu sulfide microdroplets: evidence from LA-ICP-MS analysis of sulfides in the Skaergaard Intrusion, east Greenland. Contributions to Mineralogy and Petrology 170, 1-26.

Holwell, D.A., McDonald, I., Butler, I.B., 2011. Precious metal enrichment in the Platreef, Bushveld Complex, South Africa: Evidence from homogenized magmatic sulfide melt inclusions. Contributions to Mineralogy and Petrology 161, 1011-1026.

Junge, M., Wirth, R., Oberthür, T., Melcher, F., Schreiber, A., 2015. Mineralogical siting of platinum-group elements in pentlandite from the Bushveld Complex, South Africa. Mineralium Deposita 50, 41-54.

Kamenetsky, V.S., Maas, R., Fonseca, R.O.C., Ballhaus, C., Heuser, A., Brauns, M., Norman, M.D., Woodhead, J.D., Rodemann, T., Kuzmin, D.V., Bonatti, E., 2013. Noble metals potential of sulfide-saturated melts from the subcontinental lithosphere. Geology 41, 575-578.

Kamenetsky, V.S., Park, J.-W., Mungall, J.E., Pushkarev, E.V., Ivanov, A.V., Kamenetsky, M.B., Yaxley, G.M., 2015. Crystallization of platinum-group minerals from silicate melts: Evidence from Cr-spinel–hosted inclusions in volcanic rocks. Geology 43, 903-906.

Kamenetsky, V.S., Zelenski, M., Gurenko, A., Portnyagin, M.V., Ehrig, K., Kamenetsky, M., Churikova, T., Feig, S., 2017. Silicate-sulfide liquid immiscibility in modern arc basalt (Tolbachik volcano, Kamchatka): Part II. Composition, liquidus assemblage and fractionation of the silicate melt. Chemical Geology (accepted).

Kerr, A., Leitch, A.M., 2005. Self-destructive sulfide segregation systems and the formation of high-grade magmatic ore deposits. Economic Geology 100, 311-332.

Košler, J., 2001. Laser-ablation ICPMS study of metamorphic minerals and processes, in: Sylvester, P.J. (Ed.), Laser-ablation in the earth sciences: principles and application. Mineralogical Association of Canada, pp. 185–202.

Longerich, H.P., Jackson, S.E., Gunther, D., 1996. Laser ablation inductively coupled plasma mass spectrometric transient signal data acquisition and analyte concentration calculation. Journal of Analytical Atomic Spectrometry 11, 899-904.

Meisel, T., Moser, J., 2004. Reference materials for geochemical PGE analysis: new analytical data for Ru, Rh, Pd, Os, Ir, Pt and Re by isotope dilution ICP-MS in 11 geological reference materials. Chemical Geology 208, 319-338.

McDonough, W.F., Sun, S.-s., 1995. The composition of the Earth. Chemical Geology 120, 223-253.

Mungall, J.E., 2002. Kinetic controls on the partitioning of trace elements between silicate and sulfide liquids. Journal of Petrology 43, 749-768.

Mungall, J.E., Brenan, J.M., 2014. Partitioning of platinum-group elements and Au between sulfide liquid and basalt and the origins of mantle-crust fractionation of the chalcophile elements. Geochimica et Cosmochimica Acta 125, 265-289.

Mungall, J.E., Su, S., 2005. Interfacial tension between magmatic sulfide and silicate liquids: Constraints on kinetics of sulfide liquation and sulfide migration through silicate rocks. Earth and Planetary Science Letters 234, 135-149.

Naldrett, A.J., 1997. Key factors in the genesis of Noril'sk, Sudbury, Jinchuan, Voisey's bay and other world-class Ni-Cu-PGE deposits: Implications for exploration. Australian Journal of Earth Sciences 44, 283-315.

Naldrett, A.J., 2004. Magmatic sulfide deposits: Geology, geochemistry and exploration. Springer-Verlag, Berlin Heidelberg.

Naldrett, A.J., 2010. Secular variation of magmatic sulfide deposits and their source magmas. Economic Geology 105, 669-688.

Nikulin, A., Levin, V., Carr, M., Herzberg, C., West, M., 2012. Evidence for two upper mantle sources driving volcanism in Central Kamchatka. Earth and Planetary Science Letters 321-322, 14-19.

Pagé, P., Barnes, S.J., 2016. The influence of chromite on osmium, iridium, ruthenium and rhodium distribution during early magmatic processes. Chemical Geology 420, 51-68.

Pagé, P., Barnes, S.J., Bedard, J.H., Zientek, M.L., 2012. In situ determination of Os, Ir, and Ru in chromites formed from komatiite, tholeiite and boninite magmas: Implications for chromite control of Os, Ir and Ru during partial melting and crystal fractionation. Chemical Geology 302, 3-15.

Park, J.W., Campbell, I.H., Eggins, S.M., 2012. Enrichment of Rh, Ru, Ir and Os in Cr spinels from oxidized magmas: Evidence from the Ambae volcano, Vanuatu. Geochimica et Cosmochimica Acta 78, 28-50.

Patten, C., Barnes, S.J., Mathez, E.A., 2012. Textural variations in MORB sulfide droplets due to differences in crystallization history. Canadian Mineralogist 50, 675-692.

Portnyagin, M., Bindeman, I., Hoernle, K., Hauff, F., 2007. Geochemistry of primitive lavas of the Central Kamchatka Depression: magma generation at the edge of the Pacific Plate, in:

Eichelberger, J., Gordeev, E., Izbekov, P., Kasahara, M., Lees, J. (Eds.), Volcanism and subduction: the Kamchatka region, pp. 199-239.

Portnyagin, M., Duggen, S., Hauff, F., Mironov, N., Bindeman, I., Thirlwall, M., Hoernle, K., 2015. Geochemistry of the late Holocene rocks from the Tolbachik volcanic field, Kamchatka: Quantitative modelling of subduction-related open magmatic systems. Journal of Volcanology and Geothermal Research 307, 133-155.

Pruseth, K.L., Palme, H., 2004. The solubility of Pt in liquid Fe-sulfides. Chemical Geology 208, 233-245.

Royet, J.P., 1991. Stereology: A method for analyzing images. Progress in Neurobiology 37, 433-474.

Sylvester, P.J., 2001. A practical guide to platinum-group element analysis of sulphides by laser-ablation ICPMS, in: Sylvester, P.J. (Ed.), Laser-ablation in the earth sciences: principles and application. Mineralogical Association of Canada, pp. 203-213.

Sylvester, P.J., Cabri, L.J., Tubrett, M.N., McMahon, G., Laflamme, J.H.G., Peregoedova, A., 2005. Synthesis and evaluation of a fused pyrrhotite standard reference material for platinum group element and gold analysis by laser ablation-ICPMS, in: Tormanen, T.O., Alapieti, T.T. (Eds.), 10th International Platinum Symposium "Platinum Group Elements - from genesis to benefication and environmental impact", Oulu, Finland, pp. 16-20.

Talkington, R.W., Lipin, B.R., 1986. Platinum-group minerals in chromite seams of the Stillwater complex, Montana. Economic Geology 81, 1179-1186.

Tredoux, M., Lindsay, N.M., Davies, G., McDonald, I., 1995. The fractionation of platinum-group elements in magmatic systems, with the suggestion of a novel causal mechanism. South African Journal of Geology 98, 157-167.

Volynets, A.O., Edwards, B.R., Melnikov, D., Yakushev, A., Griboedova, I., 2015. Monitoring of the volcanic rock compositions during the 2012–2013 fissure eruption at Tolbachik volcano, Kamchatka. Journal of Volcanology and Geothermal Research 307, 120-132.

Wallace, P.J., Edmonds, M., 2011. The sulfur budget in magmas: Evidence from melt inclusions, submarine glasses, and volcanic gas emissions, Reviews in Mineralogy and Geochemistry, pp. 215-246.

Wirth, R., Reid, D., Schreiber, A., 2013. Nanometer-sized platinum-group minerals (PGM) in base metal sulfides: New evidence for an orthomagmatic origin of the Merensky Reef PGE ore deposit, Bushveld Complex, South Africa. Canadian Mineralogist 51, 143-155.

Zelenski, M., Kamenetsky, V.S., Hedenquist, J., 2016. Gold recycling and enrichment beneath volcanoes: A case study of Tolbachik, Kamchatka. Earth and Planetary Science Letters 437, 35–46.

Zhang, Y., 2015. Toward a quantitative model for the formation of gravitational magmatic sulfide deposits. Chemical Geology 391, 56-73.

Zhang, Y., Ni, H., Chen, Y., 2010. Diffusion data in silicate melts, Reviews in Mineralogy and Geochemistry, pp. 311-408.

Figure captions

Fig. 1. Map of the Tolbachik volcano and the 1941 eruptive cone with an adjacent lava flow and scoria field.

Fig. 2. Compositions of the 1941 rocks compared to other Tolbachik rocks and Kamchatka volcanic rocks. (a) Total alkali vs. SiO_2 diagram. (b) K_2O vs. MgO diagram. Numbers in (b) denote two distinct trends for Tolbachik rocks: 1- middle-K rocks; 2 – high-K rocks. Lavas from the 2012-2013 eruption form a short separate trend (3). Data are from Churikova et al., 2015b; Portnyagin et al., 2007; Volynets et al., 2015.

Fig. 3. Reflected light photomicrographs demonstrating textures of sulfide globules entrapped in Tolbachik olivine phenocrysts: (a) homogeneous texture; (b) fine-grained texture inherited from high-temperature exsolution of Ni-rich sulfide phase (‘MSS’, white patches) interspersed with Cu-rich phase (‘ISS’, yellow); (c) coarse-grained globule composed of approximately equal amounts of ‘MSS’ and ‘ISS’. The sulfide solid solutions are represented

by low-temperature minerals (pyrrhotite, pentlandite, chalcopyrite and cubanite); (d) Criss-crossing lamellae of chalcopyrite and cubanite exsolved from 'ISS' with relics of 'MSS' and small patches of pentlandite. Small grains of magnetite are present inside sulfide and on the outer surface of the globule. 'MSS' – monosulfide solid solution, 'ISS' – intermediate solid solution, cb – cubanite, ccp – chalcopyrite, mgt – magnetite, pn – pentlandite, po – pyrrhotite, chr - chrome spinel.

Fig. 4. Compositions of sulfide globules in Tolbachik olivine phenocrysts. (a) Multiphase globules with textures shown in Fig. 3a-d, analyzed by EDS (grey circles) and LA-ICP-MS (green diamonds); (b) Reheated and quenched sulfide globules (red) and naturally quenched globules from sulfide swarms (blue) analyzed by EDS. Sulfide swarms of hundreds to thousands of small (< 10 μm) globules in single olivine crystals. All analyses mostly plot within the FeS-0.5NiS-0.5CuS ternary. Compositional field of quenched globules is shown in (a) for comparison.

Fig. 5. Noble metal nuggets in olivine-hosted sulfide globules. (a) BSE image of a typical sulfide globule composed of fine quenched intergrowth of 'MSS' and 'ISS' with abundant nuggets of dominantly Au, Pt, Pd-Pt and Pd_3Te ($Pd_{20}Te_7$) compositions scattered over the exposed surface as shown on panels (b, c); (d, e) Reflected light and BSE images of the sulfide globule composed of 'ISS' and pentlandite, with numerous nuggets containing Pd, Te, Pt, Au, Pb and Bi. Nuggets are mainly confined to the phase boundary between 'ISS' and pentlandite, as shown in the close-up BSE image (f). Abbreviations as in Fig. 3.

Fig. 6. Noble metal nuggets on sulfide globule surfaces. Nuggets comprised of Pt, Pd, Au, Pb, Te and Bi. Note that neighboring nuggets can be compositionally diverse.

Fig. 7. Back-scattered electron image (a), phase map (b) and X-ray element maps of sulfide globules with nuggets of three different PGE minerals (c-e). The globule contains 18 grains of Pd-Pt alloys with different Pd:Pt ratios, Cu-Pt-Rh sulfide, Ni-rich phase 'MSS' and Cu-rich phase 'ISS'. Scanning electron microscopy was performed using Versa 3D Dual Beam SEM /

FIB (FEI) instrument equipped with a field emission gun (FEG) at an accelerating voltage of 10 kV, 10 mm working distance and 12 hours of mapping time. Chemical analysis was carried out using APOLLO X Silicon Drift Detector (SDD) and TEAM software.

Fig. 8. Representative time-resolved laser ablation signals (y axis, counts per second) recorded for selected elements (masses) in sulfide globules from 1941 Tolbachik olivine crystals. Some globules are characterized by distinct metal-rich phases ("nuggets"), containing, for example, Au, Au-Pt and Pt (a, c, d), Ag, Ag-Au, Au-Pt-Bi (g) and Pd-Pt-Au-Bi (a). Note analytical data for the globules with highest abundances of Pt-Pd (e) and Rh-Os-Ir (f), and most depleted in PGE and Au, but most enriched in Re (h). See text for details.

Fig. 9. Frequency distribution histograms for logarithms of element concentrations (Pd, Os, total PGE and total chalcophile elements; concentrations of each element are normalized to 100%) measured in Tolbachik sulfide globules.

Fig. 10. Binary variation diagrams for elements in sulfide globules. (a-e) Noble metals have significant inter-correlations after excluding outliers, suggesting similar concentration mechanisms. The outliers probably represent nuggets (particles of IPGE and Au) entrapped from the silicate melt. (f) Zero correlation of moderately abundant chalcophile element (Zn) and low abundant Pt; the plot demonstrates saturation of sulfide liquid in zinc at a nearly constant level (150 ± 50 ppm) whereas the concentration of Pt varies over 3.5 orders of magnitude. Globules with fine-grained, intermediate and coarse textures are shown by different symbols. Note that globule textures have no effect on measured concentrations of noble metals. The outliers were not used for calculating coefficients of determination (R^2).

Fig. 11. Graphical representation of all measured concentrations of Au, PGE and selected chalcophile elements in Tolbachik sulfides. Samples are arranged in order of increasing gold concentrations. Areas of bubbles are proportional to concentrations of metals. Chalcophile elements Zn and Cd demonstrate roughly constant concentrations in the majority of the samples. Ranges of Au and PGE concentrations are 3-4 orders of magnitude. The highest

concentrations of Ru, Rh, Os and Ir in sample #8-9 and Au in sample #2-6 do not correlate with other elements (compare with Fig. 10). Despite anomalous concentrations of the IPGE in the sample # 8-9, no nuggets were observed under electron microscope or in time-resolved lased ablation spectrum (Fig. 6f).

Fig. 12. Nugget in silicate melt embayment containing all six platinum-group elements. (a) Melt embayment in an olivine (Fo_{83}), unpolished crystal. (b) A small 1.5x3 μm bubble on the boundary of the embayment, bright particles inside the bubble are mainly composed of Ru, Rh, Pd, Os, Ir and Pt; Cu and Fe oxides are also present. (c) EDS spectrum of the nugget shown in (b) with labeled peaks. emb – melt embayment, ol – olivine. a, b – SEM BSE images. See main text and Supplementary materials for details.

Fig. 13. Chondrite (McDonough and Sun, 1995) – normalized concentrations of noble metals in Tolbachik sulfides. (a) individual sulfide globules (gray lines), the selected globule #8-9 with anomalously high IPGE content (blue), mean sulfide composition (red) and bulk rock composition (black). (b) Comparison of mean Tolbachik sulfide composition (red) and average sulfide composition from some world-class magmatic sulfide deposits (Naldrett, 1997).

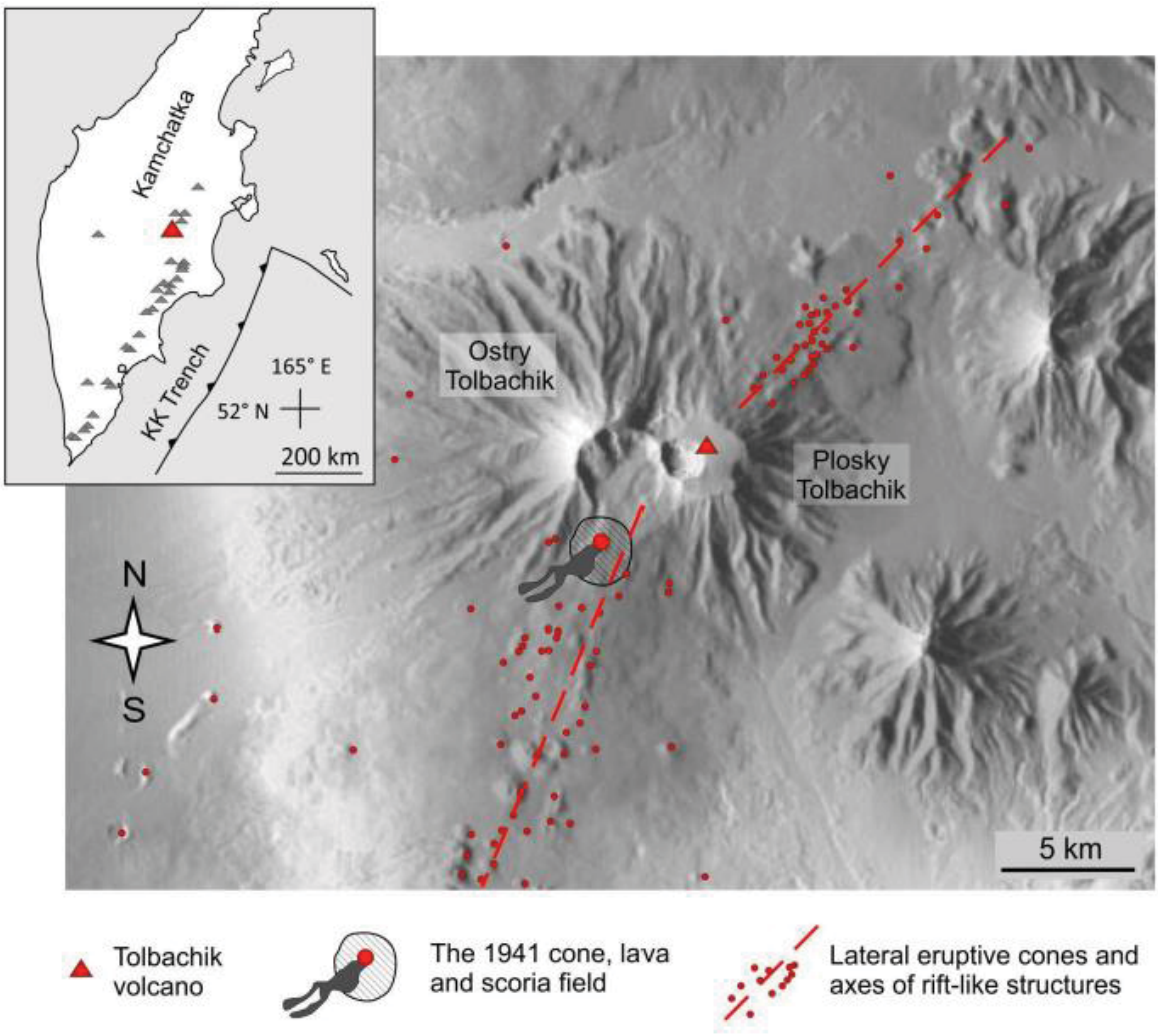

Fig. 1

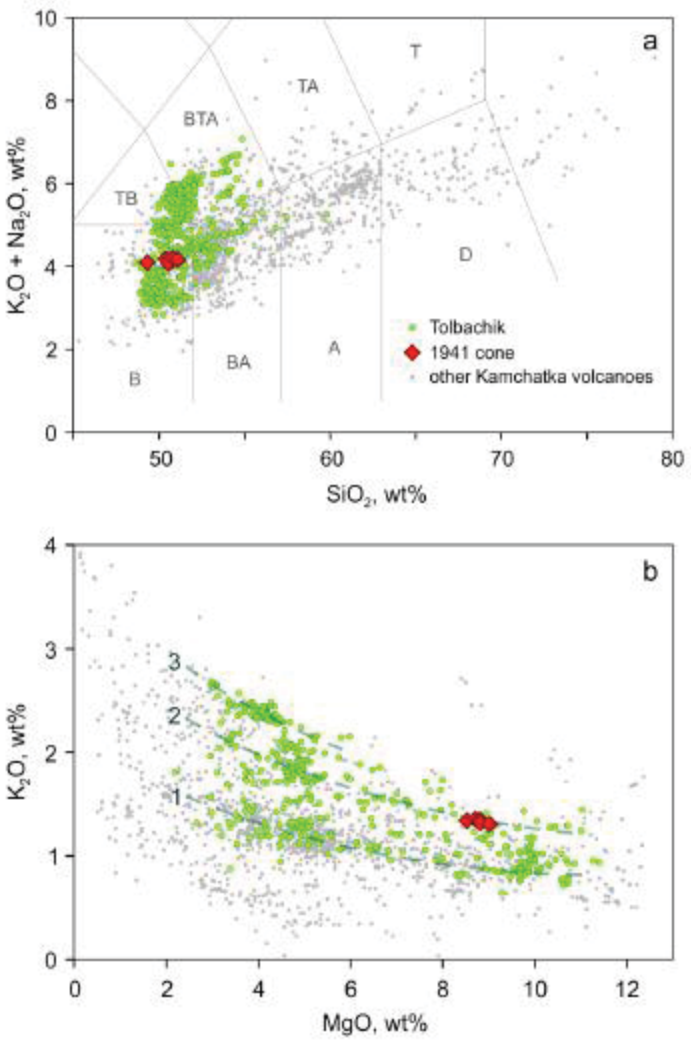

Fig. 2

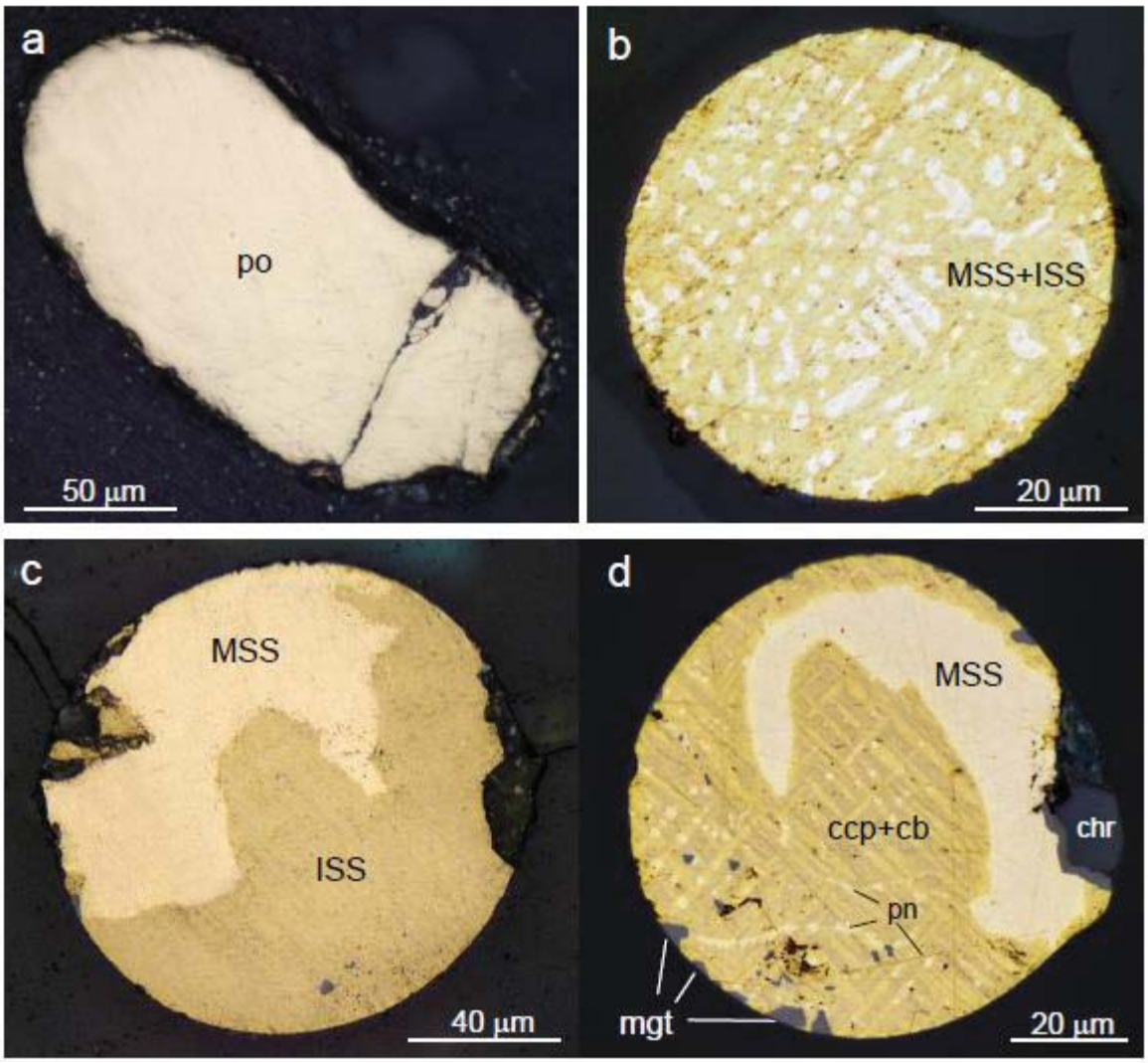

Fig. 3

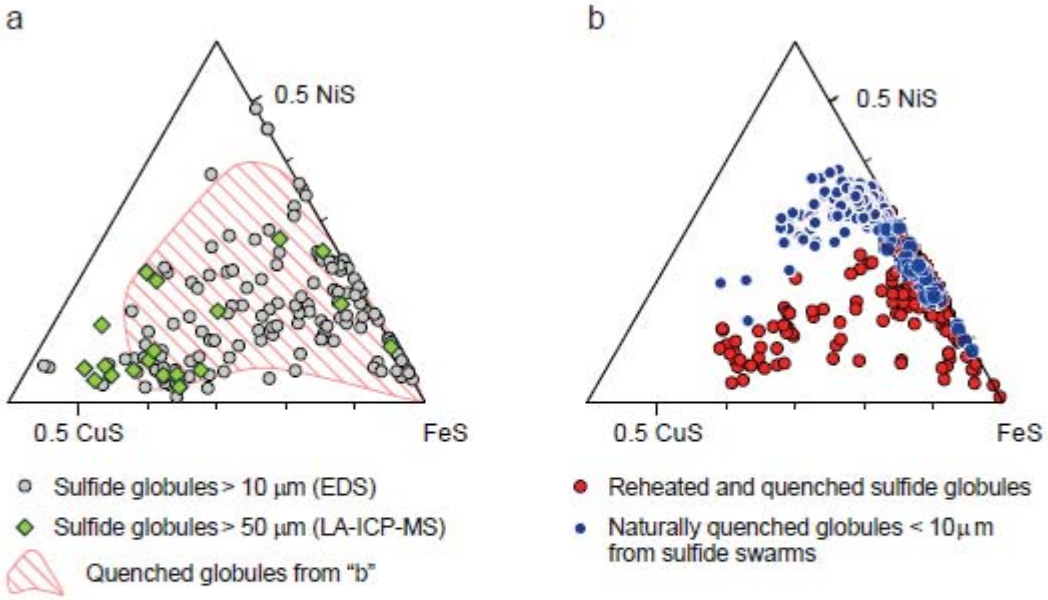

Fig. 4

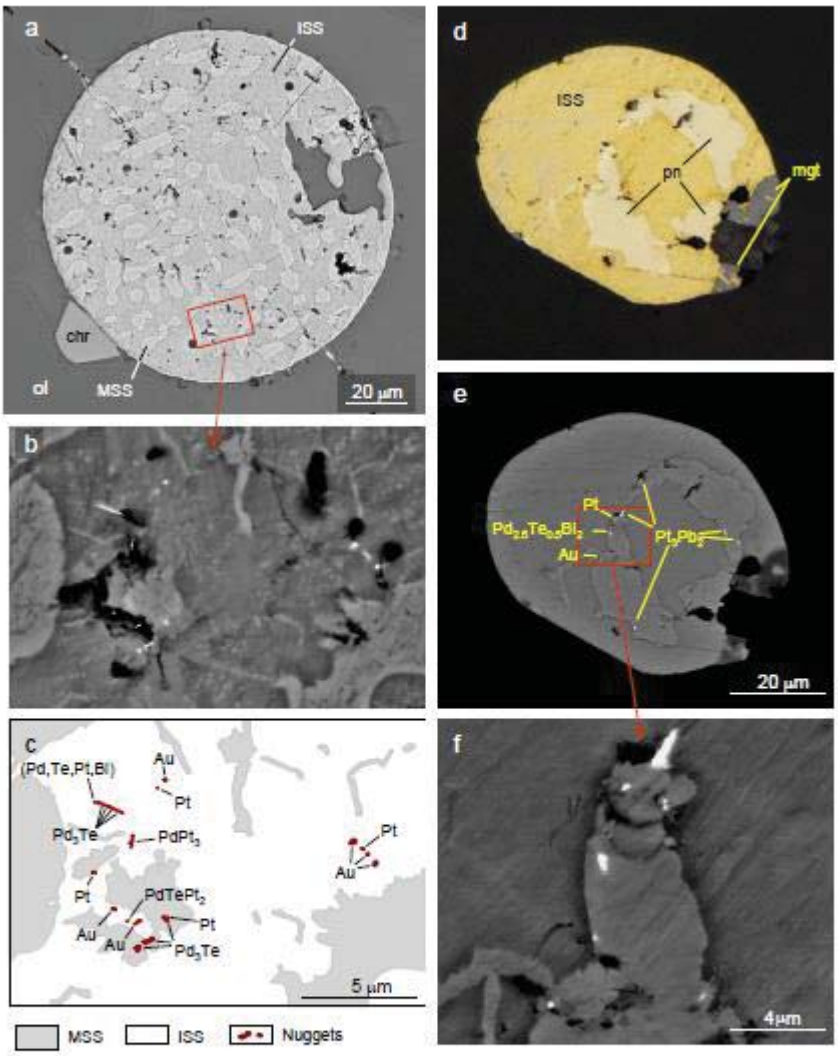

Fig. 5

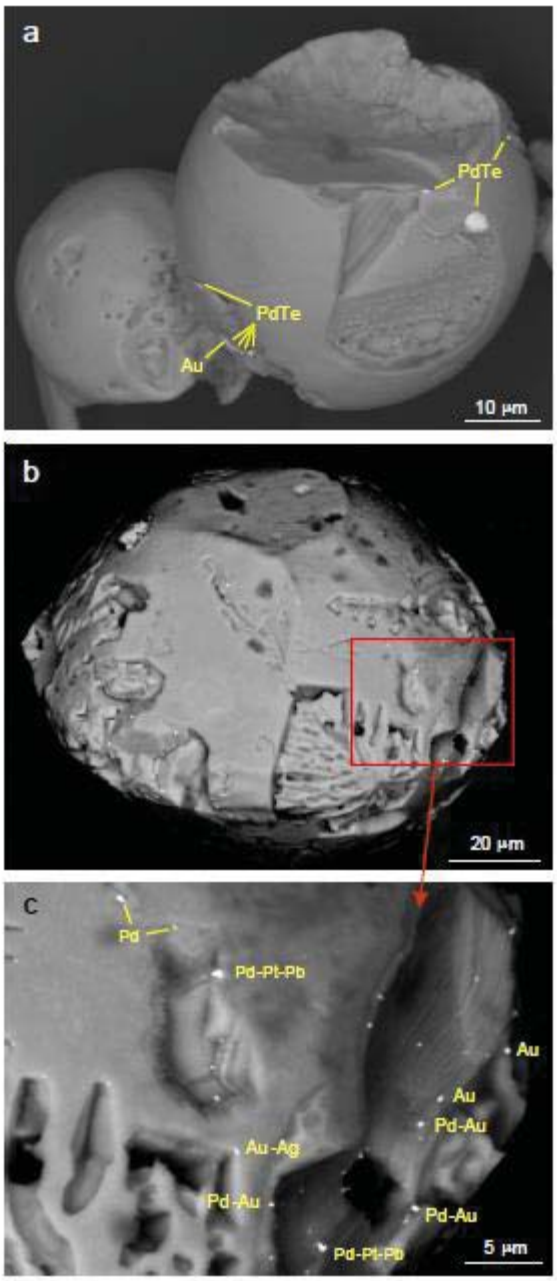

Fig. 6.

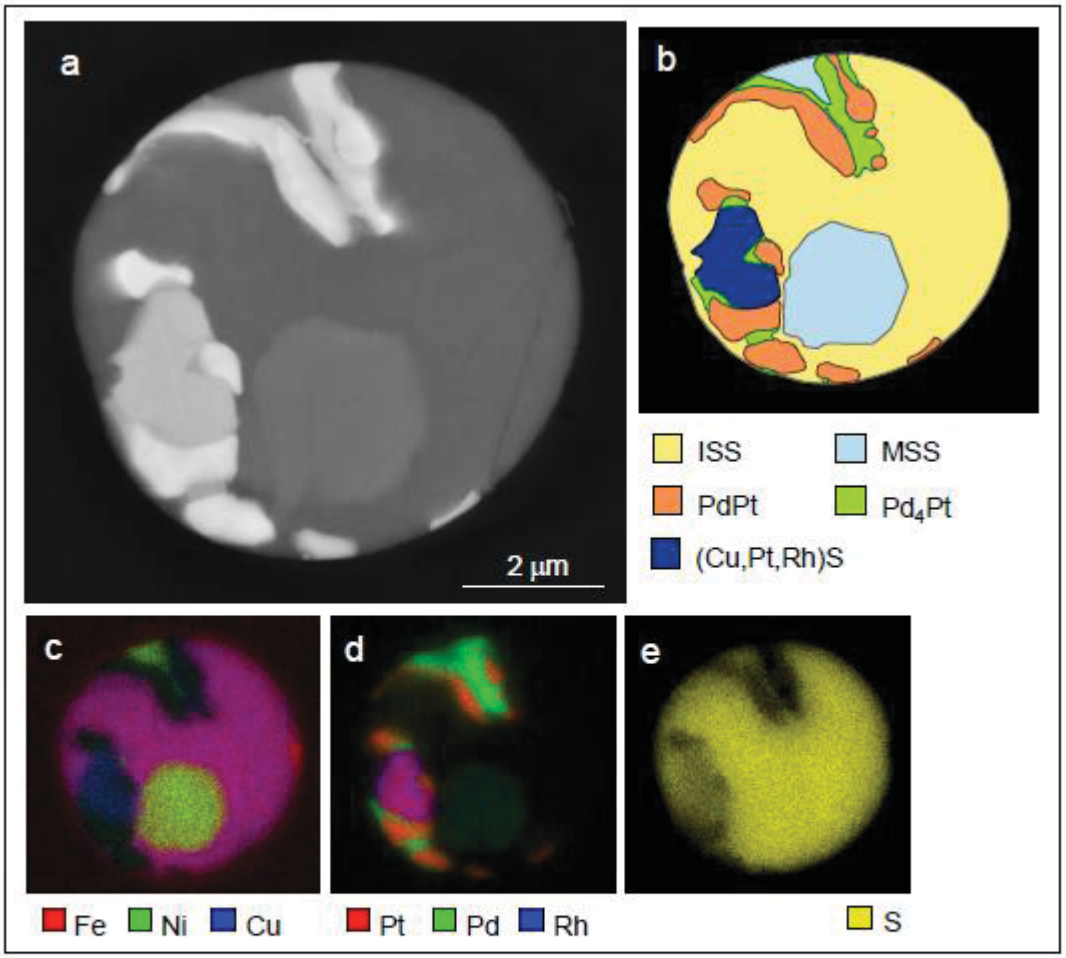

Fig. 7

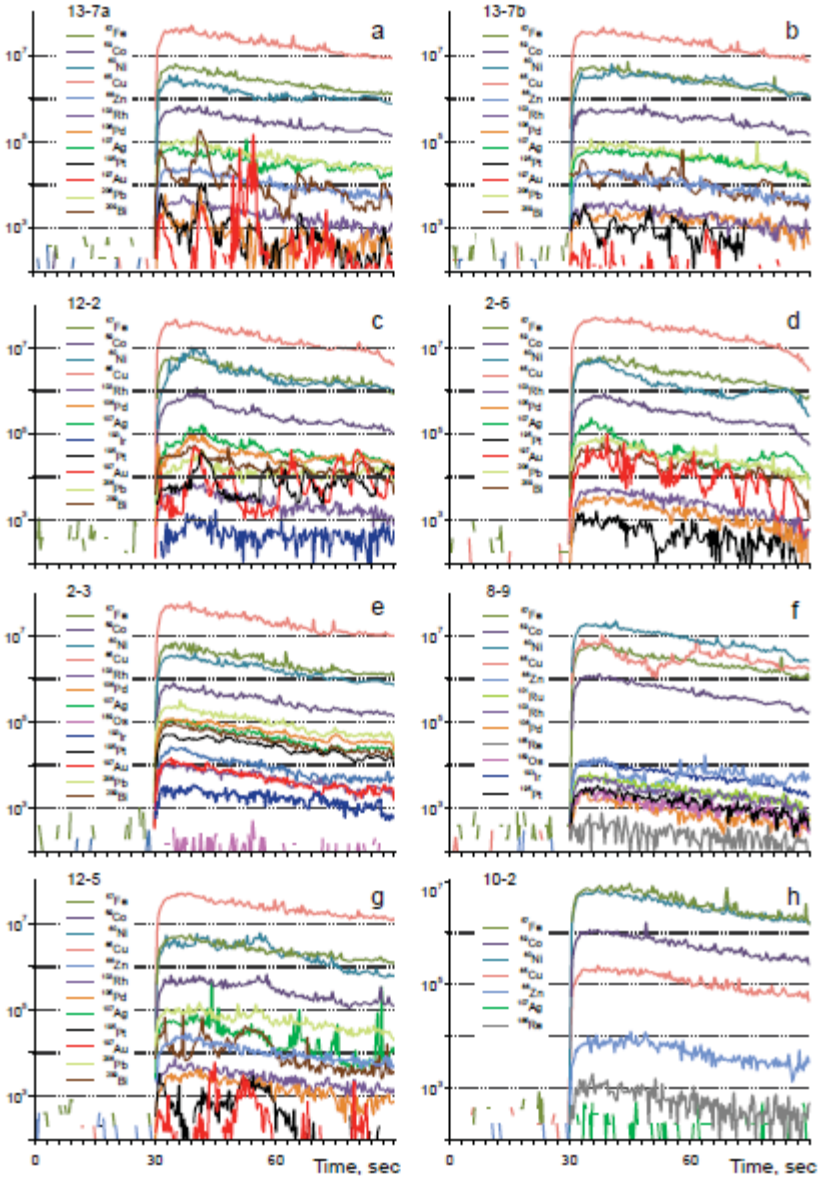

Fig. 8

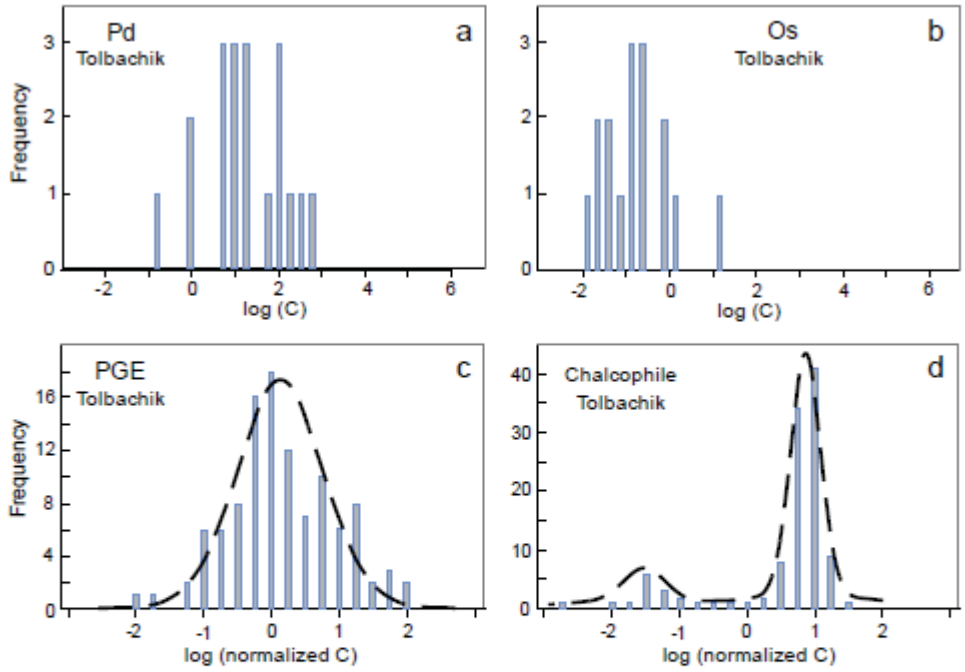

Fig. 9.

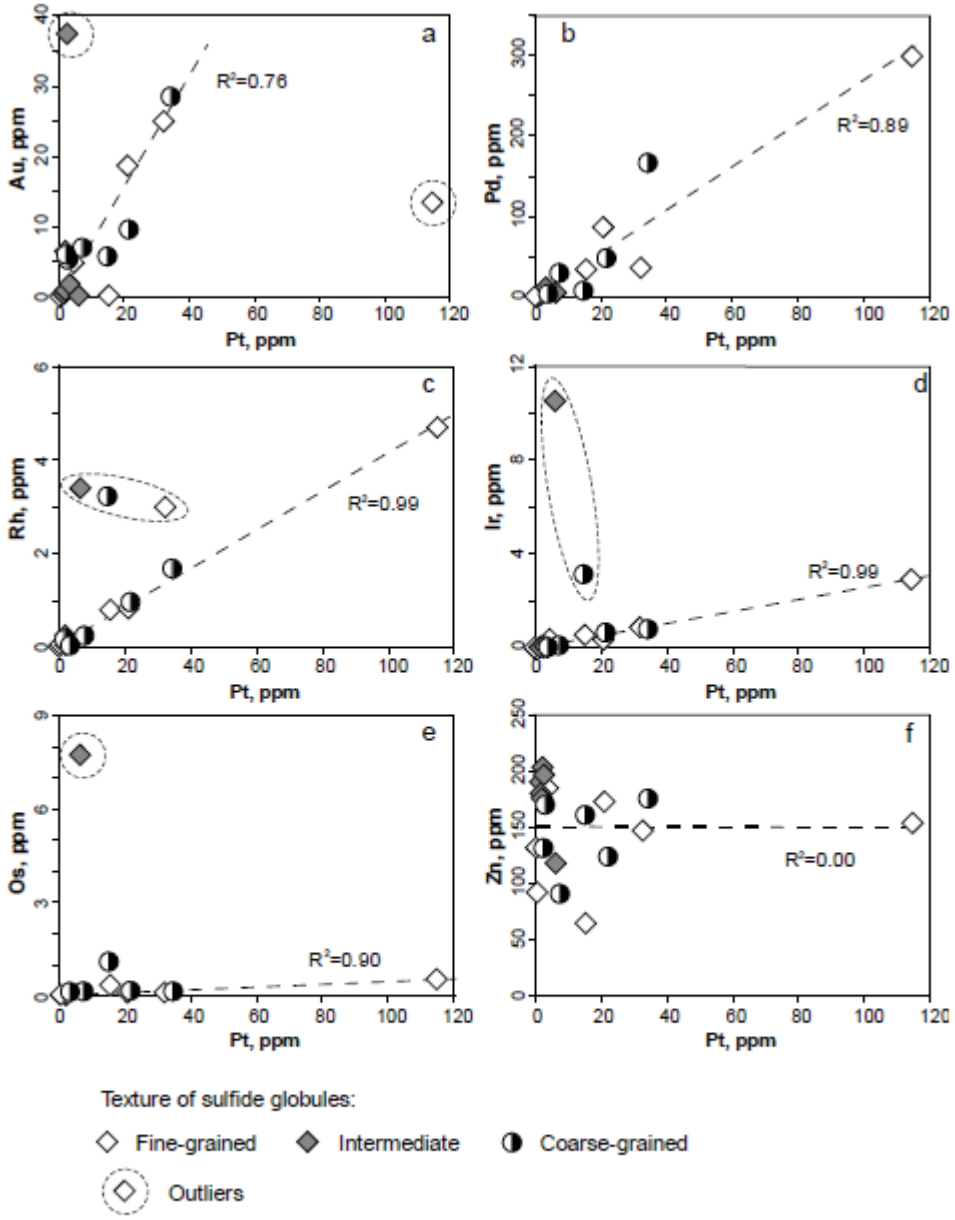

Fig. 10

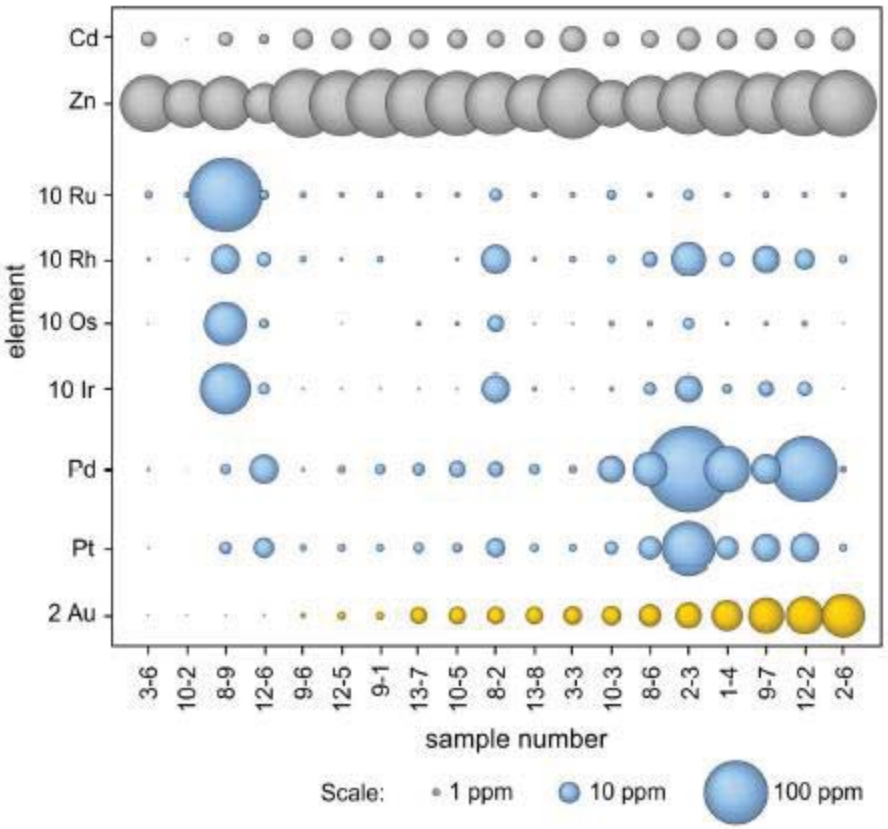

Fig. 11

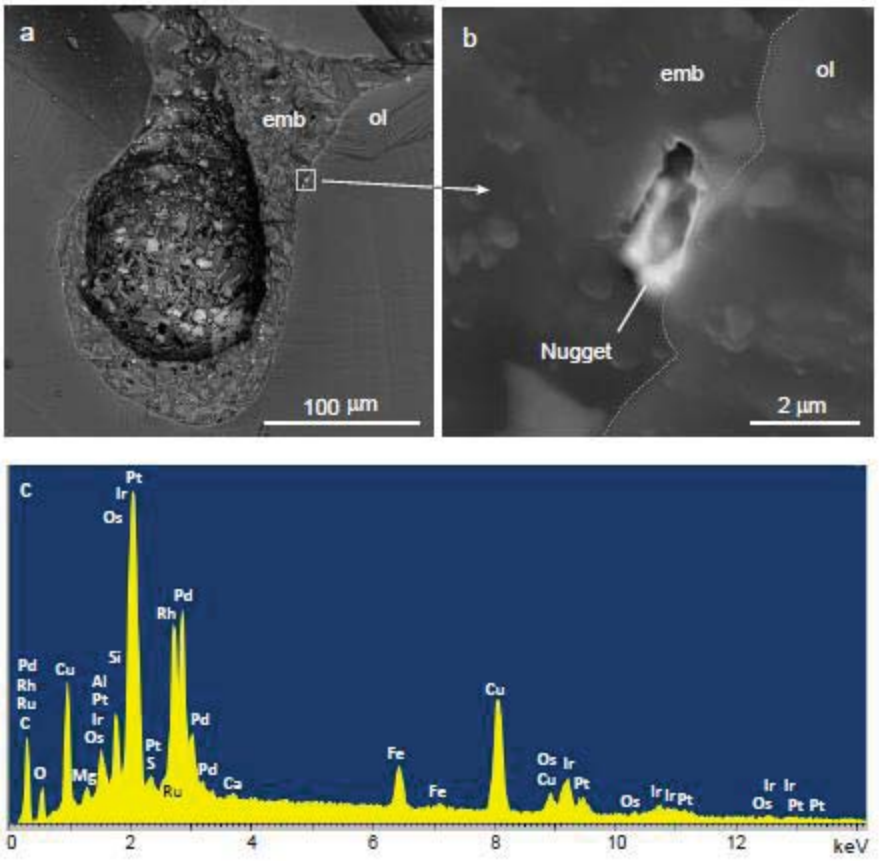

Fig. 12

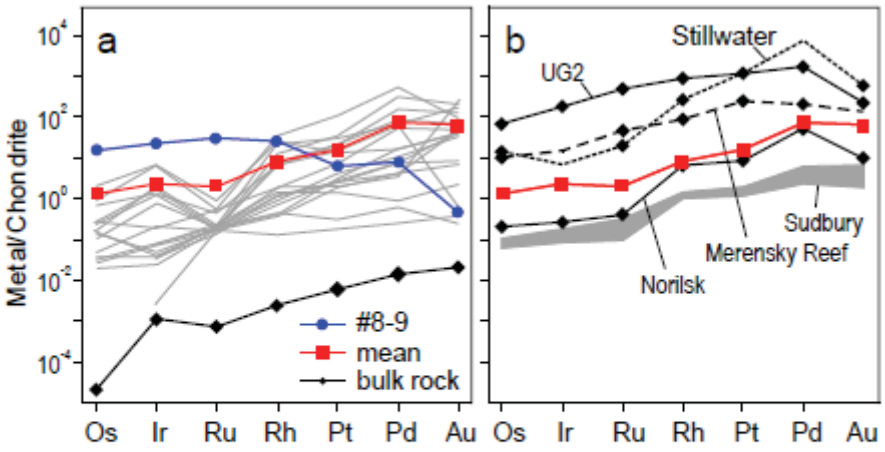

Fig. 13

Table 1. Major oxides and chalcophile element abundances in 1941 Tolbachik basalt.

Element (oxide)	Tol-1	Tol-2	Tol-4	Portnyagin et al., 2015	Churikova et al., 2015	Average for the 1941 basalt (published data *and references*)
			wt%			
SiO_2	50.83	51.0	50.56	50.4	50.53	50.66
TiO_2	1.24	1.23	1.2	1.25	1.27	1.24
Al_2O_3	14.9	15.0	14.7	14.6	14.6	14.8
FeO	9.8	9.7	9.6	9.19	9.87	9.63
MnO	0.18	0.18	0.18	0.17	0.18	0.18
MgO	8.8	8.8	9.0	8.51	8.89	8.80
CaO	9.8	9.8	9.8	9.75	10.05	9.84
Na_2O	2.8	2.8	2.8	2.85	2.8	2.81
K_2O	1.4	1.3	1.3	1.34	1.39	1.35
P_2O_5	0.38	0.38	0.36	0.38	0.38	0.38
			ppm			
Co	42.5	43.1	42.0	41		42
Ni	165	132	143	128	231	160
Cu	170	166	159	165	281	188
Zn	87	87	81	56.6	72	77
Ag						0.021 *ref. 1*
Cd	0.087	0.108	0.083		0.10	0.095
Te						0.004 *refs. 2, 3*
Pb	3.5	3.7	3.4	2.7	3.5	3.4
Bi						0.037 *ref. 2*
			ppb			
Ru	0.54	0.48	0.34			0.45
Rh	0.32	0.33	0.29			0.31
Pd	7.55	7.8	8.09			7.8
Re						0.47 *refs. 4, 5*
Os						0.0010 *refs. 4, 5*
Ir	0.76	0.72	0.52			0.67
Pt	6.37	6.0	5.81			6.1
Au	2.93	2.85	2.67			2.8

Concentrations of Ag, Te, Re, Os and Bi were taken from literature; numbers of references are given in parentheses: 1 – Flerov et al. (1984); 2 – Wedepohl (1995); 3 – Yi et al. (1995); 4 – Alves et al. (2002); 5 – Dosseto et al. (2003). See Supplementary Table 3 for full list of trace elements in the 1941 Tolbachik basalt.

Table 2. Compositions of sulfide globules measured by rastered EDS and by LA-ICP-MS (recalculated to 100% sulfide, wt%).

Sample#	Mean D, µm	Texture	Mg# of host olivine	S	Fe	Ni	Cu	S	Fe	Ni	Cu
				EDS				LA-ICP-MS			
1-4	250	Fine	89.0	32.13	44.79	3.38	19.70	34.30	42.70	3.41	19.50
2-3	160	Fine	84.8	33.22	35.44	3.23	28.10	34.30	34.50	2.85	28.30
2-6	120	Intermediate	88.2	33.51	33.48	4.63	28.39	34.30	33.30	2.26	30.10
3-3	200	Intermediate	86.8	33.98	39.46	2.47	24.10	36.50	38.00	2.80	22.50
3-6	75	Fine	89.5	37.55	46.18	15.07	1.20	38.50	44.60	15.40	1.28
8-2	50	Coarse	88.1	33.37	33.50	10.53	22.61	34.70	31.90	14.10	19.10
8-6	60	Coarse	88.4	34.51	31.12	9.73	24.64	37.50	29.40	7.96	25.10
8-9	90	Intermediate	90.4	36.17	41.50	16.25	6.08	38.70	40.00	16.60	4.53
9-1	80	Intermediate	86.0	34.40	41.69	1.49	22.42	37.70	39.40	1.46	21.30
9-6	90	Intermediate	88.7	34.56	41.92	2.87	20.65	36.60	39.20	2.81	21.20
9-7	100	Fine	88.8	33.17	35.17	4.31	27.34	34.20	33.40	3.90	28.30
10-2	250	Fine	89.0	38.23	55.61	6.16	0.00	36.40	57.40	5.77	0.17
10-3	80	Coarse	89.4	34.74	31.96	14.37	18.94	36.90	32.20	12.60	18.00
10-5	140	Coarse	88.3	35.17	35.70	4.80	24.33	34.50	37.10	5.43	22.80
12-2	80	Coarse	87.5	33.83	34.86	6.28	25.03	36.70	35.90	4.37	23.00
12-5	120	Intermediate	87.2	33.94	31.85	4.78	29.43	35.80	30.90	3.52	29.70
12-6	110	Fine	88.0	37.81	45.35	8.50	8.33	38.80	48.70	9.89	2.40
13-7	130	Fine	83.5	33.92	37.42	3.67	25.00	35.80	35.50	3.32	25.30
13-8	130	Coarse	89.0	37.13	39.51	12.09	11.27	39.50	37.80	9.11	13.50

Table 3. Nugget compositions and statistics.

System	Number of cases	Phase composition* (number of cases)
	Single metals	
Ag	3	Ag_2S
Pt	23	Pt
Au	18	Au
Pb	11	PbS
	Binary systems	
Pd-Au	16	Au_6Pd (5) Au_3Pd (4) Au_2Pd (5) Variable (2)
Pd-Te	23	$Pd_{20}Te_7$ (5)** PdTe (18)
Pd-Pt	8	Variable from 2:1 to 1:10
PdPb	2	PdPb
Ag-Au	11	Variable from 1:0.4 to 1:4.5
Te-Pt	2	$PtTe_3$
Pt-Au	7	PtAu (4) Pt_2Au_{11} (3)
Pt-Pb	7	Pt_3Pb_2
Pt-Bi	3	Variable from 1:1.5 to 1:4.6
AuPb	1	AuPb
PbBi	3	Pb_2Bi
	Ternary systems	
Pd-Ag-Au	2	Variable
Ag-Au-Pb	1	
Pd-Au-Pb	1	
Pt-Au-Pb	1	
Ag-Pt-Au	2	$(AgPt)Au_2$
Pd-Te-Pt	8	$(Pt,Pd)_3Te_8$ (2) Variable (6)
Pd-Te-Au	1	$Pd_9Au_9Te_2$
Pd-Te-Bi	2	Variable
Pt-Te-Bi	4	Variable
Pd-Pt-Au	11	Variable
Pd-Pt-Pb	13	$PdPt_4Pb$ (2) $(PdPt)_2Pb$ (11)
Pd-Pt-Bi	4	$(Pt,Pd)_2Bi_3$
Pd-Au-Bi	1	
Ag-Au-Bi	1	$Ag_9Au_9Bi_2$
Pt-Pb-Bi	2	Pt_3Pb_2Bi
	Complex systems	
Pd-Te-Pt-Bi	3	
Pd-Te-Pb-Bi	1	
Pd-Pt-Au-Pb	6	
Pd-Ag-Pt-Au	1	
Pd-Ag-Pt-Au-Bi	1	
Ag-Pd-Pt-Pb	1	
Ag-Pd-Pt-Au-Pb	1	
Pt-Au-Bi-Te	1	

Table 4. Concentrations of major and trace elements in Tolbachik sulfides (ppm) and basic statistics.

Slf #	D, μm	Texture	S	Fe	Co	Ni	Cu	Zn	Ru	Rh	Pd
1-4	250	Fine	343000	427000	957	34100	195000	172	0.137	0.834	86.9
2-3	160	Fine	343000	345000	1080	28500	283000	154	0.405	4.71	**299**
2-6	120	Intermediate	343000	333000	1030	22600	301000	180	0.135	0.244	1.88
3-3	200	Intermediate	365000	380000	1200	28000	225000	203	0.104	0.155	2.17
3-6	75	Fine	385000	446000	2150	154000	12800	132	0.191	0.0594	0.354
8-2	50	Coarse	347000	319000	2080	141000	191000	161	0.632	3.22	9
8-6	60	Coarse	375000	294000	1150	79600	251000	125	0.119	0.954	48.7
8-9	90	Intermediate	387000	400000	2020	166000	45300	118	**22.3**	3.4	4.38
9-1	80	Intermediate	377000	394000	1500	14600	213000	192	0.161	0.147	4
9-6	90	Intermediate	366000	392000	1510	28100	212000	190	0.175	0.184	0.537
9-7	100	Fine	342000	334000	1220	39000	283000	148	0.162	3	35.7
10-2	250	Fine	364000	574000	2060	57700	1650	92.3	0.126	0.0172	0.0894
10-3	80	Coarse	369000	322000	1560	126000	180000	91.4	0.381	0.239	29.6
10-5	140	Coarse	345000	371000	1210	54300	228000	170	0.135	0.0539	9.97
12-2	80	Coarse	367000	359000	1070	43700	230000	176	0.133	1.68	**173**
12-5	120	Intermediate	358000	309000	909	35200	297000	175	0.119	0.0521	2.26
12-6	110	Fine	388000	487000	2040	98900	24000	64.9	0.316	0.806	34.4
13-7	130	Fine	358000	355000	1090	33200	253000	184	0.126	< dl	5.88
13-8	130	Coarse	395000	378000	1610	91100	135000	131	0.115	0.0915	4.21
Min			342000	294000	909	14600	1650	64.9	0.104	0.0172	0.0894
Max			395000	574000	2150	166000	301000	203	22.3	4.71	299
Max/min			1.15	1.96	2.37	11.4	**182**	3.13	214	273	**3350**
Median			365000	371000	1220	43700	213000	161	0.137	0.242	5.88
Mean			364000	380000	1440	67100	187000	151	1.36	1.1	39.6
Mean/median			0.996	1.02	1.19	1.54	0.882	0.932	**9. 93**	**4.56**	**6.74**

Table 4 (continued)

Sample	Ag	Cd	Te	Re	Os	Ir	Pt	Au	Pb	Bi	Total Au+PGE
1.4	211	16.9	174	0.0355	0.0532	0.362	21.1	18.8	95.1	25.4	128
2.3	157	21.4	132	0.0401	0.466	2.95	**115**	13.4	288	34.5	**436**
2.6	126	21.2	102	< dl	0.00963	0.0112	1.92	37.5	93.2	17.6	41.7
3.3	125	27.8	80.4	0.0324	0.0183	0.0165	2.26	6.57	110	19.3	11.3
3.6	0.349	8.91	3.38	0.12	0.0148	< dl	0.317	0.0349	0.497	0.0811	0.97
8.2	94.4	12.3	60.5	0.0283	0.983	3.15	15	5.76	101	28	37.7
8.6	110	12	76.8	0.0983	0.128	0.598	21.7	9.58	92.2	24.3	81.7
8.9	3.02	7.56	2.85	0.511	**7.73**	**10.5**	6.3	0.0653	1.61	0.101	54.7
9.1	51	17.3	42.1	0.0126	< dl	0.0157	2.39	1.21	44.2	6.49	7.9
9.6	106	16.6	41.6	0.039	< dl	0.0336	1.47	0.334	81.7	10.7	2.7

9.7	136	17.4	104	0.0513	0.088	0.884	32.2	25	94	17.1	97
10.2	0.355	0.164	0.133	0.963	< dl	0.00115	< dl	0.0527	0.141	0.00342	**0. 29**
10.3	90.3	9.77	23.5	0.502	0.134	0.0845	7.49	7.01	63.5	8.29	45
10.5	102	14.5	66.7	0.0333	0.0704	0.0226	3.22	5.67	136	16.7	19.1
12.2	177	14.6	332	0.0767	0.135	0.797	34.5	28.6	46.8	20.1	239
12.5	101	16.8	56.4	0.0204	0.0134	0.034	2.04	0.941	175	11.6	5.5
12.6	20.3	3.45	1.02	0.154	0.325	0.548	15.5	0.0855	0.249	< dl	52
13.7	136	14.6	79.4	0.044	0.0763	0.0177	3.93	4.94	157	15	15
13.8	65.9	13.1	44.8	0.256	0.0246	0.0949	2.82	6.03	72.4	11.7	13.4
Min	0.349	0.164	0.133	0.0126	0.00963	0.00115	0.317	0.0349	0.141	0.00342	0.29
Max	211	27.8	332	0.963	7.73	10.5	115	37.5	288	34.5	436
Max/min	604	169	2500	76.7	803	**9110**	362	1080	2050	**10100**	1520
Median	102	14.6	60.5	0.0476	0.0822	0.0897	5.12	5.76	92.2	15.8	38
Mean.	95.4	14	74.9	0.168	0.642	1.12	16	9.03	86.9	14.8	68
Mean/median	0.931	0.961	1.24	3.52	**7. 81**	**12. 5**	3.13	1.57	0.943	0.936	1.8

Table 5. Semiquantitative EDS analyses of PGE-containing "micro-nugget".

Element	Analytic line	Spectrum #3			Spectrum #7			Only PGE, wt% (average)
		wt%	2 σ	at%	wt%	2 σ	at%	
O	K_series	10.7	2.36	38.8	10.49	1.08	38.71	
Mg	K_series	0.67	0.13	1.59	0.51	0.06	1.25	
Al	K_series	1.26	0.13	2.7	1.33	0.06	2.92	
Si	K_series	2.26	0.13	4.67	2.32	0.06	4.88	
S	K_series	0.51	0.12	0.92	0.5	0.06	0.93	
K	K_series	0.2	0.12	0.3	0.25	0.06	0.38	
Ca	K_series	0.29	0.12	0.42	0.39	0.06	0.58	
Fe	K_series	4.35	0.23	4.52	3.98	0.11	4.2	
Cu	K_series	21.62	0.53	19.75	22.76	0.26	21.15	
Ru	L_series	0.51	0.43	0.29	0.77	0.2	0.45	1.0
Rh	L_series	15.52	0.61	8.76	13.1	0.28	7.52	23.0
Pd	L_series	11.49	0.59	6.27	11.37	0.28	6.31	18.4
Os	L_series	2.99	1.22	0.91	2.83	0.59	0.88	4.7
Ir	M_series	20.9	0.72	6.31	20.97	0.34	6.44	33.6
Pt	M_series	12.73	0.79	3.79	11.26	0.37	3.41	19.3
Totals		105.98		100	102.84		100	
PGE		64.14			60.3			100.00

Highlights

- Primitive arc basalt magma represents 1941 eruption of Tolbachik volcano, Kamchatka
- Silicate-sulfide melt immiscibility is recorded as melt inclusions in olivine Fo_{86-92}
- Sulfide melt inclusions are highly variable in Ni/Cu and PGE, Ag, Te, Au, Pb and Bi
- Micron-sized particles of Au, Pt, Au-Pd and Pd-Te are abundant in sulfide globules
- Tolbachik sulfide melts are compositionally similar to sulfides in magmatic deposits